引用格式：刘超，沈晨阳，李昕，等. 2026. 右江盆地巴马台地下石炭统沉积旋回记录对晚古生代冰期主幕启动的响应[J]. 沉积学报. DOI: 10.14027/j.issn.1000-0550.2026.017
Liu Chao, Shen Chenyang , Li Xin, et al. 2026. Lower Carboniferous Sedimentary Cycles in the Bama Platform of the Youjiang Basin: Responses to the Onset of the Main-phase of the Late Paleozoic Ice Age[J]. Acta Sedimentologica Sinica. DOI: 10.14027/j.issn.1000-0550.2026.017.
DOI: 10.14027/j.issn.1000-0550.2026.017 CSTR: 32268.14/j.cjxb.62-1038.2026.017

右江盆地巴马台地下石炭统沉积旋回记录对晚古生代冰期主幕启动的响应

刘超，沈晨阳，李昕，戚俊俊
河南理工大学资源环境学院，河南焦作 454000

摘　要 【目的】早石炭世中晚期是地球构造古地理、气候、海洋环境和生态系统的重大变革期，厘定它们的发生时序对于揭示重大气候突变期地球各圈层、系统相互作用机理意义重大。为精确约束晚古生代大冰期主幕启动时间，【方法】以华南右江盆地巴马孤立台地水峒剖面下石炭统都安组为研究对象，通过系统的沉积微相及相序分析，构建了海侵—海退层序，并恢复了右江盆地早石炭世中晚期相对海平面变化历史。【结果】在水峒剖面维宪阶中部至谢普霍夫阶顶部共识别出 12 种沉积微相，可合并为 4 种沉积相组合类型，分别为局限台地相组合、开阔台地相组合、台地边缘颗粒滩相组合和上斜坡相组合。水峒剖面维宪阶上部和谢普霍夫阶共发育 7 个三级海侵—海退层序和至少 26 个四级海侵—海退旋回。【结论】右江盆地高频、高幅海平面变化初现于 Aleksinian-Mikhailovian 期之交，与低纬其他远程响应指标记录一致，表明晚古生代大冰期主幕启动于该时期。

关键词　右江盆地；晚古生代大冰期；沉积微相；海侵—海退层序；有孔虫带

第一作者　刘超，男，1989 年出生，教授，碳酸盐岩沉积学、地层学，E-mail: liuchao661030@126.com

中图分类号：P534.4；P532　**文献标志码**：A　**文章编号**：1000-0550（2026）00-0000-00

0　引言

早石炭世是地球构造古地理、气候、海洋环境和生态系统的重大变革期（王向东等，2019）。北方欧美古陆与南方冈瓦纳古陆于早石炭世开始碰撞（海西造山运动），在赤道附近形成中央造山带（Nance *et al.*，2010）。伴随造山带的隆升、风化剥蚀和维管植物的扩张（Goddéris *et al.*，2017；Chen *et al.*，2018；要乐等，2023），中高纬冈瓦纳古陆上发育了大规模的冰川运动（Isbell *et al.*，2003；Fielding *et al.*，2023），地球随即进入显生宙以来持续时间最长、规模最大的冰室气候（即晚古生代大冰期；Eyles，1993；Montañez and Poulsen，2013）。

晚古生代大冰期的开始、持续时间及发育规模通常由近源指标和远程响应指标约束（Frank *et al.*，2008）。近源指标是指冈瓦纳古陆上保存的与冰川活动直接相关的沉积记录（Isbell *et al.*，2003；Jones and Fielding，2004；Fielding *et al.*，2008），包括块状—层状杂

收稿日期：2026-02-05；**收修改稿日期**：2026-04-10
基金项目：国家自然科学基金项目（42572135, 42172120）

砾岩、含坠石泥岩、韵律层、冰蚀岩面、砾石擦痕—棱面、软沉积褶皱—断裂、U 型谷等。但这些近源记录往往缺乏精确的地层时代标定（Isbell *et al.*，2003；Heckel，2008）；同时由于后期冰川消融—增长过程对早期冰川记录的改造和侵蚀，近源沉积地层的完整性亦难以保证（Smith and Read，2000）。因此，更多学者关注低纬地区有连续生物化石带约束的海相或海陆交互相沉积序列，期望借助远程响应指标获取更加详尽的晚古生代冰室气候演变信息。远程响应指标主要包括低纬沉积序列中所含的旋回层（Fielding，2021；Heckel，2023）、高频、高幅海平面变化信号（Rygel *et al.*，2008；Ahern and Fielding，2021）及地球化学信号（如 C-O 同位素；Joachimski *et al.*，2006；郄文昆等，2010；Chen *et al.*，2013，2016b；仲钰天等，2023）。通过大陆克拉通盆地滨浅海层序界面和沉积旋回的识别，可推测海平面变化的频度和幅度。一般认为，高频、高幅（<0.5 Myr；>20 m）海平面变化可反映受冰川活动的影响，而低幅海平面波动则可能与非冰川因素有关（Rygel *et al.*，2008）。石炭纪至早二叠世低纬沉积序列中普遍发育了高频、高幅海侵—海退旋回（如刘本培等，1994；李儒峰等，1997；张海军等，2006；Eros *et al.*，2012；Liu *et al.*，2018），代表冰川型全球海平面变化，受冈瓦纳冰盖冰量变化的控制和调节（Heckel，2008）。伴随冈瓦纳冰盖的增长与消融，全球古海洋海水化学组成和碳循环也发生了相应改变，并影响到沉积物的 C-O 同位素组成（$\delta^{13}C$ 和$\delta^{18}O$；Buggisch *et al.*，2008）。通常，在排除成岩作用影响后，冰期和暖期分别对应碳酸盐或磷酸盐矿物高和低的 C-O 同位素比值（Grossman and Joachimski，2022）。具体表现为，$\delta^{18}O$ 升高（降低）指示高纬冰盖增长（消融）、储存（释放）更多富 ^{16}O 的淡水；$\delta^{13}C$ 升高（降低）反映有机碳埋藏速率或海洋表面初始生产力增大（减小），大气 pCO_2 下降（升高），全球气候变冷（转暖）（Mii *et al.*，1999；Chen *et al.*，2016a；Yao *et al.*，2022）。

近源指标和部分远程响应指标表明，冈瓦纳古陆冰川活动在泥盆纪末和石炭纪初（杜内期中期）就已出现（Buggisch *et al.*，2008；Lakin *et al.*，2016；Caputo and dos Santos，2020），并伴随剧烈的海洋环境和生态系统变化（Yao *et al.*，2015，2020；Kaiser *et al.*，2016；Maharjan *et al.*，2018；Chen *et al.*，2021；Qie *et al.*，2023；Zhong *et al.*，2025）。不过这两幕冰川活动均缺乏高频高幅海平面变化远程响应记录（Fielding，2021），它们通常被认为是独立的、短暂的（< 1~2 Ma）冰期事件（Fielding and Frank，2015；Montañez，2022）。冈瓦纳古陆上更为广泛的、持续的陆地冰川活动（即晚古生代大冰期主幕）始于早石炭世晚维宪期（Soreghan *et al.*，2019；Montañez，2022），但其精确的启动时间尚不明晰。虽然中晚维宪期—早谢普霍夫期冰川活动近源记录广泛分布于南美洲沉积盆地中（Montañez，2022；Fielding *et al.*，2023），晚古生代大冰期主幕的精确启动时间需要远程指标约束（如高频、

高幅海平面变化信号的初现；Fielding，2021）。

前人已在低纬沉积序列中广泛识别出了高频、高幅海平面变化信号（Smith and Read，2000；Wright and Vanstone，2001；Al-Tawil and Read，2003；Gallagher *et al.*，2006；Bishop *et al.*，2009；Giles，2009；Waters and Condon，2012；Fielding and Frank，2015；Kabanov *et al.*，2016；Cózar *et al.*，2022，2023；Hounslow *et al.*，2024），但其初现时间却存在显著差异（尽管绝大多数研究记录的初现时间为 Asbian 晚期）。这真的客观地反映晚古生代大冰期不存在统一的陆地冰川活动启动时间吗？还是少数研究对地层年代解释不准确导致的假象？这些问题的存在严重阻碍了重大气候突变期地球系统科学研究。华南板块泥盆纪末至石炭纪一直位于古特提斯洋东侧（Scotese，2021），不受海西造山运动的直接影响，其沉积记录可能更具有代表性。虽然前人已识别出 Asbian 期（Liu *et al.*，2015）、Brigantian 中期（Chen *et al.*，2019）和维宪期—谢普霍夫期之交（Chen *et al.*，2016b；Huang *et al.*，2020）显著的冰期海平面下降事件，但对维宪阶中上部缺乏高时间分辨率的沉积旋回研究。近几年，笔者通过系统的有孔虫和牙形石生物地层研究，已在华南右江盆地建立起早石炭世中晚期可进行跨区域对比的、统一的年代地层格架（Liu *et al.*，2023a，b，c，2026a）。基于此，本文对右江盆地巴马孤立台地水峒剖面都安组中上部进行精细的沉积微相和海侵—海退旋回研究，同时结合全球最新的年代地层研究成果，精确对比其他远程响应指标，从而厘定晚古生代大冰期主幕的精确启动时间、探讨冰期启动机制。

1　地质背景

华南板块由扬子陆块和华夏陆块在新元古代早期沿江南造山带拼合而成（Cawood *et al.*，2018）。早石炭世，华南板块处于东古特提斯洋近赤道地区（图 1A；Scotese，2021）。右江盆地位于华南板块西南部（冯增昭等，1999），传统观念认为，该盆地以三大断裂系统（即师宗—弥勒断裂、紫云—丹池断裂和凭祥—南宁断裂）和八布缝合带作为边界（Zeng *et al.*，1995；Cai and Zhang，2009；Yang *et al.*，2012）。但最近 Wang *et al.*（2020）对此提出了质疑，他们认为这些断裂带可能主要形成于中生代或新生代，盆地的范围应该根据其泥盆纪裂谷阶段原始的古地理格局来定义。这样一来，右江盆地的范围明显扩大，包括所有被扬子古陆、华夏古陆和云开古陆所环绕的碳酸盐岩台地、硅质碎屑岩台地及深水盆地（图 1B）。

在大地构造位置上，右江盆地地处古特提斯洋与泛大洋（即古太平洋）构造域复合带（图 1A）。与这些构造域相关的造山旋回被认为是右江盆地诞生和演化的主要驱动力（Wang *et al.*，2020）。自早泥盆世以来，东古特提斯洋分支洋的打开和扩张导致右江盆地沿被动大陆边缘

发生裂陷（Zeng *et al.*，1995；Metcalfe，2013）。其结果是，在盆地内部形成了许多孤立碳酸盐岩台地被深水盆地环绕的景象，同时在扬子古陆边缘发育了大片的连陆台地（史晓颖等，2006；Liu *et al.*，2015）。到晚二叠世—早三叠世，伴随古太平洋或东古特提斯洋分支洋的俯冲消减，以及华南板块与印支板块的碰撞，右江盆地演化为前陆盆地（Yang *et al.*，2012；杜远生等，2013；Wang *et al.*，2018，2020）。这一系列事件导致右江盆地内的孤立碳酸盐岩台地由南向北逐步被淹没（Lehrmann *et al.*，2015；Liu *et al.*，2015）。

巴马台地是右江盆地内典型的孤立碳酸盐岩台地（刘超，2014）。水峒剖面位于巴马台地北缘，主要包括都安组地层。都安组厚 434 米，沉积时代为早石炭世中维宪期至晚石炭世巴什基尔早期，由厚层状生物碎屑泥粒—颗粒灰岩、中薄层泥晶—粒泥灰岩、微生物岩和白云岩化灰岩组成（图 2；Liu *et al.*，2023a）。剖面自下而上共包括 9 个有孔虫生物化石带，分别为：下石炭统 *Pojarkovella nibelis-Endothyranopsis compressa* 带、*Cribrospira panderi-Eostaffella ikensis* 带、*Climacammina* 带、*Janischewskina delicata* 带、*Eostaffellina decurta* 带、*Bradyina cribrostomata* 带、*Eostaffellina actuosa-Eostaffellina protvaensis* 带、*Plectostaffella* 带和上石炭统 *Pseudostaffella antiqua* 带（图 3）。其中，*Plectostaffella* 带与 *Pseudostaffella antiqua* 带之间为平行不整合关系（Liu *et al.*，2023a），该沉积间断面可与其他低纬地区早—晚石炭界限附近的不整合面进行对比（Blake and Beuthin，2008；Rygel *et al.*，2008；Bishop *et al.*，2009；Eros *et al.*，2012；Chen *et al.*，2019）。

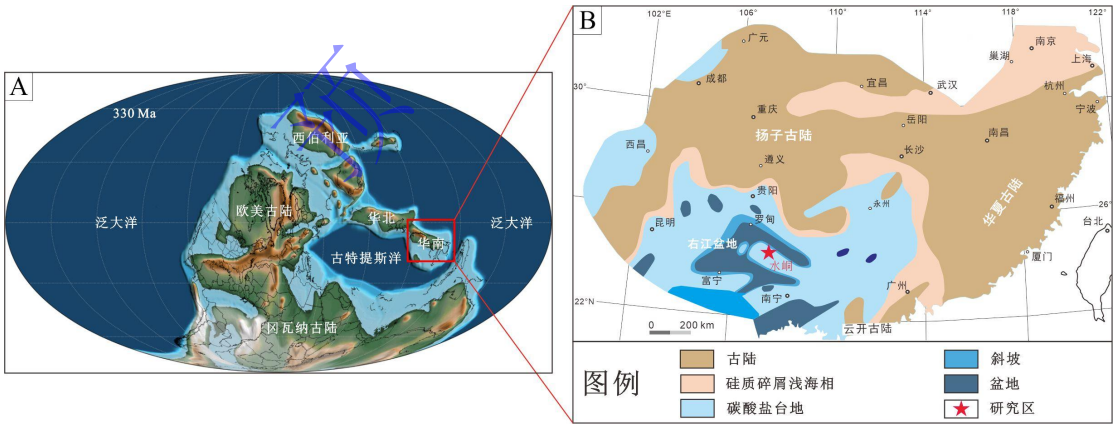

图 1 早石炭世全球和华南板块古地理图

（A）早石炭世晚期全球古地理重建图（修改自 Scotese，2021）；（B）华南板块早石炭世岩相古地理图（修改自冯增昭等，1999）

Fig. 1 Paleogeographic reconstruction maps of the globe and South China during the Early Carboniferous

(A) Global paleogeographic reconstruction map of the late Early Carboniferous (modified after Scotese, 2021); (B) Lithofacies paleogeographic map of South China during the Early Carboniferous (modified after Feng *et al.*, 1999)

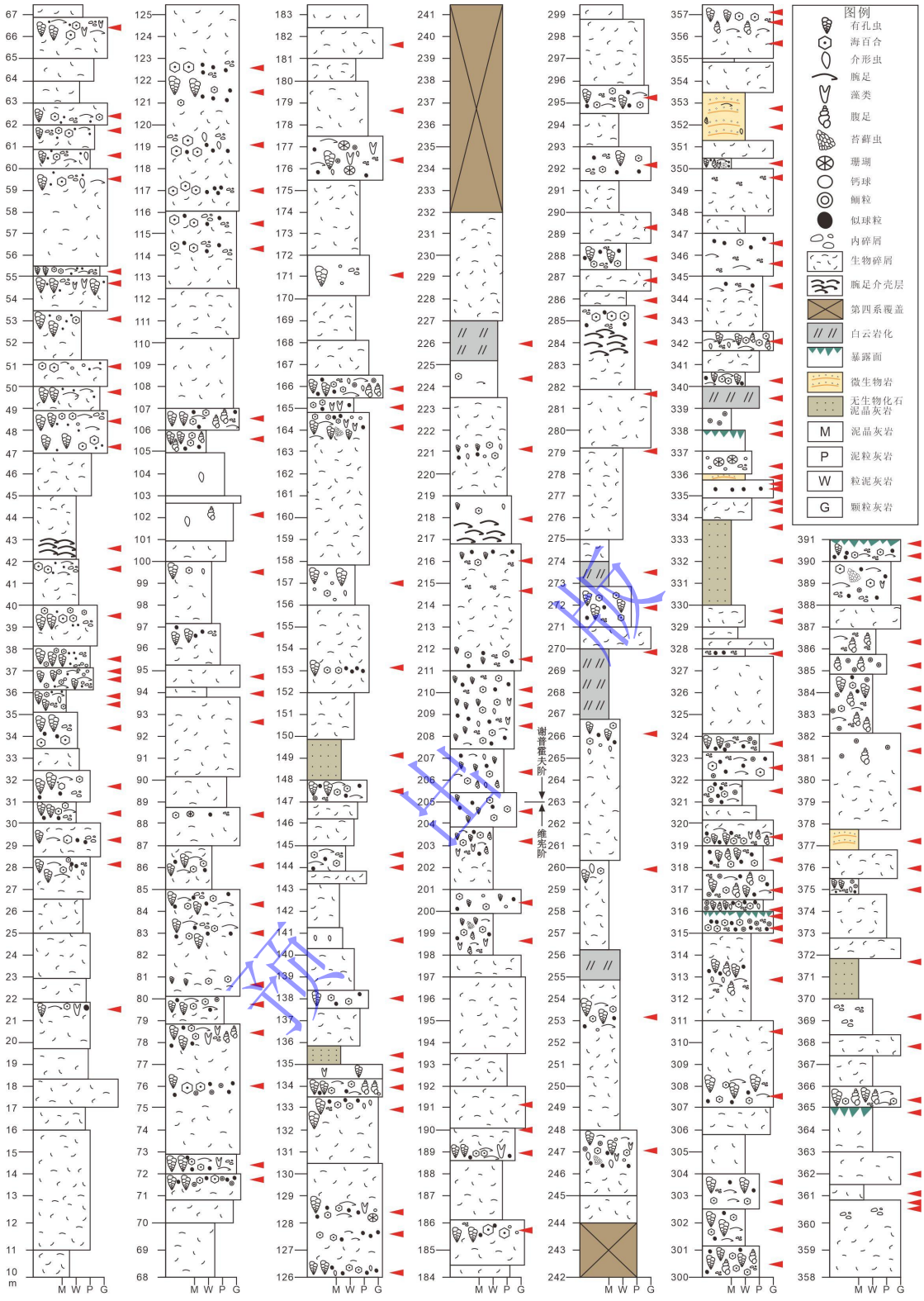

图 2 水峒剖面都安组沉积柱状图（红色箭头为采集样品位置）

Fig.2 Detailed sedimentologic log of the Du'an Formation in the Shuidong section (Red arrows indicate sampling locations)

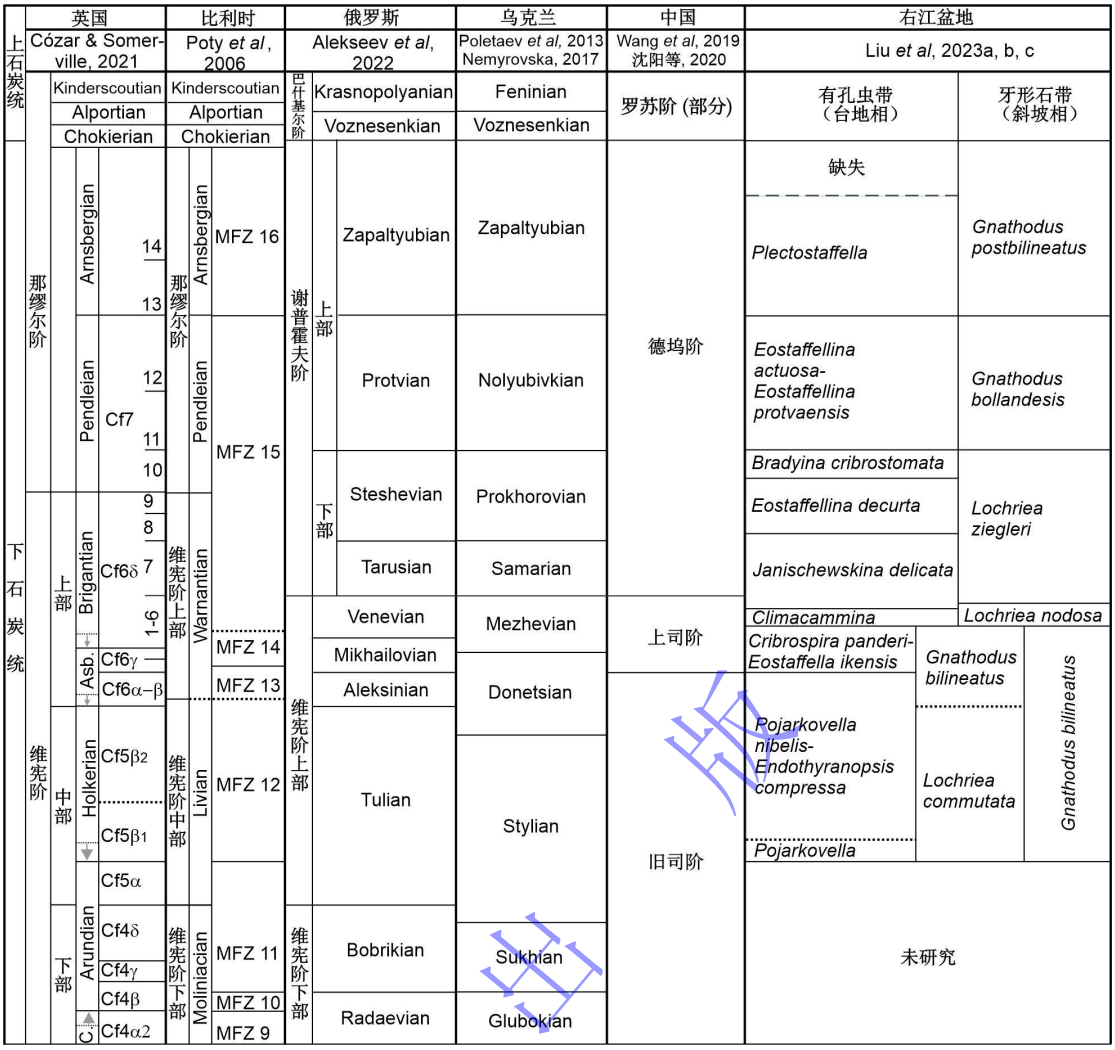

图 3 右江盆地与全球其他地区石炭系中部年代地层对比图

虚线为尚未确定的界线位置。英国年代地层引自 Cózar and Somerville（2021），比利时年代地层引自 Poty *et al*.（2006），俄罗斯年代地层根据 Alekseev *et al*.（2022），乌克兰年代地层根据 Poletaev *et al*.（2013）和 Nemyrovska（2017），中国年代地层根据 Wang *et al*.（2019）和沈阳等（2020），右江盆地有孔虫化石带与牙形石化石带引自 Liu *et al*.（2023a，b，c，2026a）。缩写含义：C.-Chadian；Asb.-Asbian

Fig. 3 A comparison chart of middle Carboniferous chronostratigraphy in the Youjiang Basin, South China, and selected global regions

Note that dashed lines indicate boundaries that have not yet been definitively established. Regional chronostratigraphy of United Kingdom is from Cózar and Somerville (2021), Belgium from Poty *et al*. (2006); Russia from Alekseev *et al*. (2022), Ukraine from Poletaev *et al*. (2013) and Nemyrovska (2017), China from Wang *et al*. (2019) and Shen *et al*. (2020), and foraminiferal and conodont biozones of Youjiang Basin from Liu *et al*. (2023a, b, c, 2026). Abbreviations: C.-Chadian; Asb.-Asbian

3 研究材料与方法

微相分析是碳酸盐沉积模式建立和古海洋沉积环境恢复的重要研究手段之一（Flügel，2010）。在水峒剖面下石炭统都安组中（*Pojarkovella nibelis-Endothyranopsis compress* 带至 *Plectostaffella* 带）共采集新鲜样品 166 件，并制作标准岩石薄片 198 件。对薄片进行系统的镜下观察、拍照，以确定岩石结构、构造及颗粒组合类型。

岩石命名依据 Dunham（1962）分类方案。薄片中的生物和非生物颗粒组分百分比含量通过对比目估图进行估算（Mathews *et al.*，1991），并按照 0%，＜1%，1%~5%，5%~20%，＞20%五个等级进行划分。通过综合分析所采样品层位的层厚、颜色、岩性、结构、构造、颗粒组分等信息，确定微相类型及其沉积环境。然后根据微相和沉积相组合堆积样式及其横向分布特征重建水峒剖面下石炭统海侵—海退沉积序列，进而恢复华南右江盆地早石炭世中晚期相对海平面变化历史。

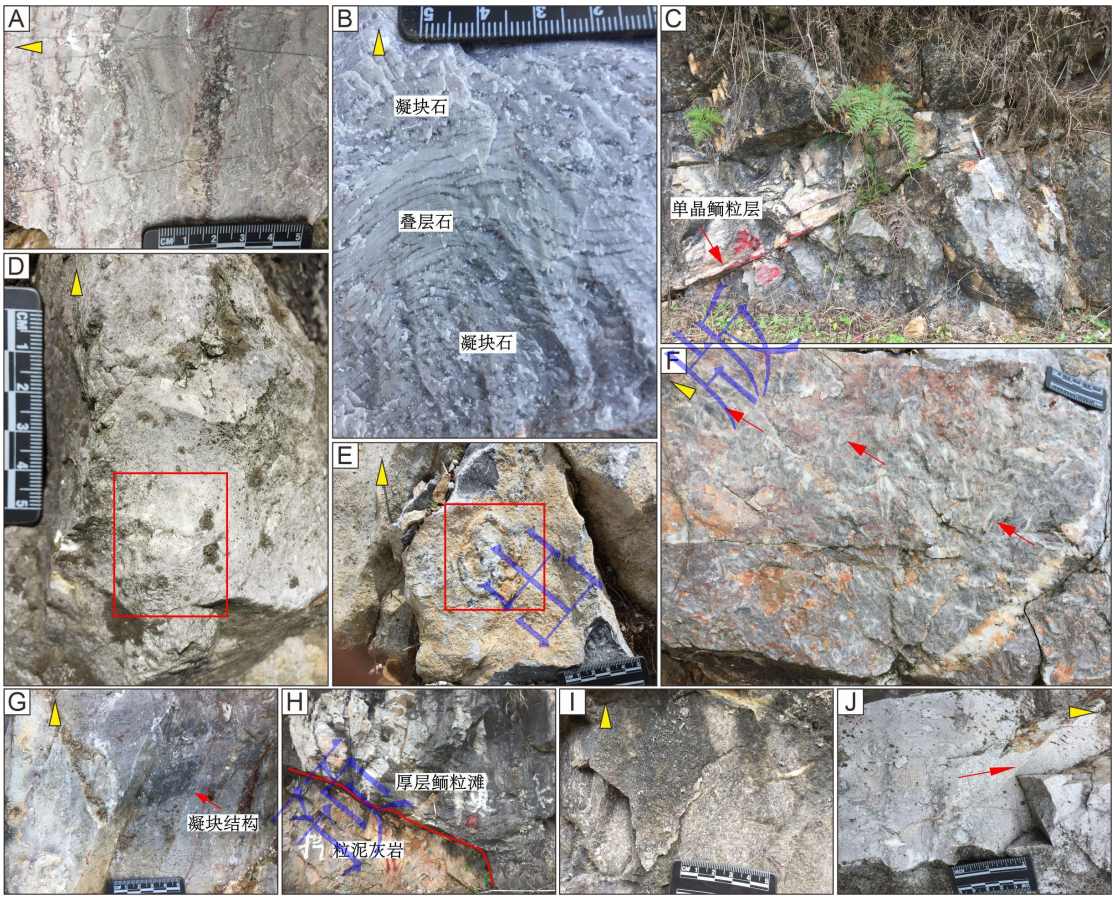

图 4 水峒剖面下石炭统都安组典型野外照片

（A）含蒸发盐矿物的微生物岩；（B）含凝块—微生物席复合组构的微生物岩；（C）30 层底部的单晶鲕粒层（红色箭头所指）；（D）含完整横板珊瑚化石（红框所示）的泥粒灰岩；（E）含完整腕足化石（红框所示）的泥粒灰岩；（F）腕足介壳层，大多数介壳凸面向上（红色箭头所示）；（G）含微生物凝块组构的粒泥灰岩（红色箭头所指）；（H）厚层鲕粒滩覆盖于潮下带粒泥灰岩之上；（I）颗粒滩相灰岩；（J）上斜坡相砾屑灰岩，具有正粒序层理（红色箭头所示）。注：黄色箭头方向指示地层顶部

Fig.4 Typical field photographs of the Lower Carboniferous Du'an Formation at the Shuidong section

(A) Microbialite containing abundant evaporite minerals; (B) Microbialite displaying both thrombolitic and stromatolitic fabrics; (C) A monocrystalline ooid layer (indicated by the red arrow) at the basal Bed 30; (D) Packstones containing whole tabulate corals (highlighted by the red box); (E) Packstones containing whole brachiopods (highlighted by the red box); (F) A brachiopod shell bed exhibiting a predominantly convex-up orientation of the shells (indicated by the red arrows); (G) Wackestones with thrombolitic fabrics (indicated by the red arrow); (H) Massive shoal oolitic grainstones overlying subtidal wackestones; (I) Shoal grainstones; (J) Upper slope rudstones with normal graded bedding. Note: Yellow arrows indicate the stratigraphic top

4 水峒剖面下石炭统沉积相分析

在水峒剖面下石炭统都安组中共识别出 12 种微相类型（用 Mf1-12 表示；表 1）。这些微相可进一步合并为 4 种沉积相组合类型，包括局限台地相组合、开阔台地相组合、台地边缘颗粒滩相组合和上斜坡相组合。

4.1 局限台地相组合

Mf1：白云岩化灰岩或白云岩。该微相主要位于旋回层顶部，包含块状白云岩和不同白云岩化程度的灰岩。其原生组分和基质大多被白云石晶体（粒径通常小于 50 μm）交代，晶体呈半自形，边界较平直（图 5A），表明其不是晚期埋藏成岩或热液成因白云石（Gregg and Sibley，1984；Warren，2000）。前人研究认为，这类白云岩或白云岩化灰岩是多期次海平面波动背景下（Lumsden and Caudle，2001），在低海平面时期通过准同生白云岩化作用叠加形成的（Ning *et al.*，2020；Hu *et al.*，2021）。白云岩化流体可能源于海平面下降后蒸发作用下形成的高盐卤水（Machel and Mountjoy，1986）。综上所述，该微相沉积于干旱的潮上带环境（宋英凡等，2024）。

Mf2：含窗格构造的泥晶—泥粒灰岩。该微相以发育较多微米级至毫米级被亮晶方解石充填的窗格构造泥晶灰岩为特征（图 5B），表明其发育于潮上带干旱环境，反映暴露后受到了大气淡水成岩作用的影响（Fügel，2010）。此外，部分层位可见含不规则纹层状窗格构造的泥粒灰岩（图 5C），其可能与不同类群蓝细菌捕获、黏结似球粒形成粗粒叠层石格架后、部分未钙化蓝细菌被分解留下孔洞有关（刘萧萧等，2025）。该微相沉积于干旱的、间歇性受潮汐作用影响的潮上带至潮间带环境（Fügel，2010；刘萧萧等，2025）。

Mf3：含蒸发盐矿物的微生物岩。该微相几乎不含生物碎屑，以发育丰富的石膏（假晶，被方解石交代）等蒸发盐矿物与凝块状/叠层状微生物组构为特征（图 4A~B，图 5D~E）。石膏等蒸发盐矿物的出现，是蒸发作用加剧，水体盐度过饱和，盐类矿物沉淀析出所致（Warren，2010）。伴随水体盐度的不断升高，后生动物逐渐较少，创造了有利于微生物生长、繁殖的环境（Riding，2000），凝块石和层状微生物席复合组构指示较低能的沉积环境（Wilson and Palmer，1992）。综上所述，该微相沉积于干旱的潮上带至潮间带环境。

Mf4：含单晶鲕粒的泥粒灰岩。该微相的特征是在沉积间断面之下发育单晶鲕粒层（图 4C，图 5F~G），其可能是先前形成的鲕粒灰岩在暴露地表后，经淋滤作用和准同生大气淡水溶蚀作用，由单晶方解石充填而成（新生变形作用；Ma *et al.*，2008；Aigbadon *et al.*，2024）。此外，在单晶鲕粒层及其之下的泥晶化鲕粒层中可见明显的植根构造（图 5F）。该微相形成

于潮上带暴露环境，鲕粒灰岩源岩则形成于受潮汐作用影响的潮间带（Wilson and Roberts，1992）。

4.2 开阔台地相组合

Mf5：富含有孔虫和海百合的泥粒灰岩。该微相以含丰富的有孔虫和海百合化石为特征（图 5H），其含量可达生物颗粒总含量的 30%以上。其次还见介形虫、腕足、腹足和藻类等生物颗粒以及似球粒和内碎屑等非生物颗粒。颗粒分选较差，磨圆度中等，表明水体能量中等（Yang *et al.*，2020）。有孔虫、海百合、腕足、腹足等生物组合通常指示开阔台地环境（Alsharhan and Kendall，2003；Youssef *et al.*，2017；Sallam *et al.*，2022）。综上所述，该微相形成于水动力条件中等的浅潮下带环境，位于正常天气浪基面之上。

Mf6：含完整化石的漂砾灰岩。该微相以发育含完整珊瑚或腕足化石的漂砾灰岩为特征（图 4D~E）。基质通常为细小的生物碎屑（包括腹足、双壳、有孔虫、藻类和海百合等）、似球粒和碳酸盐泥（图 5I），反映其处于正常天气浪基面之下较深水的低能环境中（Fügel，2010；Boboye and Okon，2014；Liu *et al.*，2018）。多样的生物组合通常代表水体营养和盐度正常的开阔海环境（Fügel，2010）。该微相沉积于开阔台地相潮下带下部环境。

Mf7：含腕足介壳的漂砾灰岩。该微相宏观上以发育腕足介壳为特征，形成介壳层（图 4F）。腕足介壳多为分离的单瓣壳、凸面向上（图 4F），基质通常为泥粒灰岩（图 6A~B），指示中等的水动力条件，其代表正常天气浪基面与风暴浪基面之间典型的风暴沉积（处于远源和近源风暴沉积之间；Butts，2005；Yao *et al.*，2016）。此外，常见的棘皮、腕足和腹足等生物组合，指示正常盐度的开阔海环境（Chesnel *et al.*，2016）。综上所述，该微相形成于开阔台地相潮下带下部环境。

Mf8：凝块状粒泥灰岩。该微相宏观上具有明显的凝块结构（图 4G），镜下除丰富的管状钙化蓝细菌和晶洞构造外（图 6C~D），还常见似球粒、内碎屑、腕足、海百合和腹足等生物与非生物碎屑颗粒，这可能是由于底栖微生物群落在生长和代谢过程中黏结碎屑颗粒并在原地沉积而成（Riding，2011）。因此，该微相形成于开阔的深水潮下带低能环境（Riding，2000）。

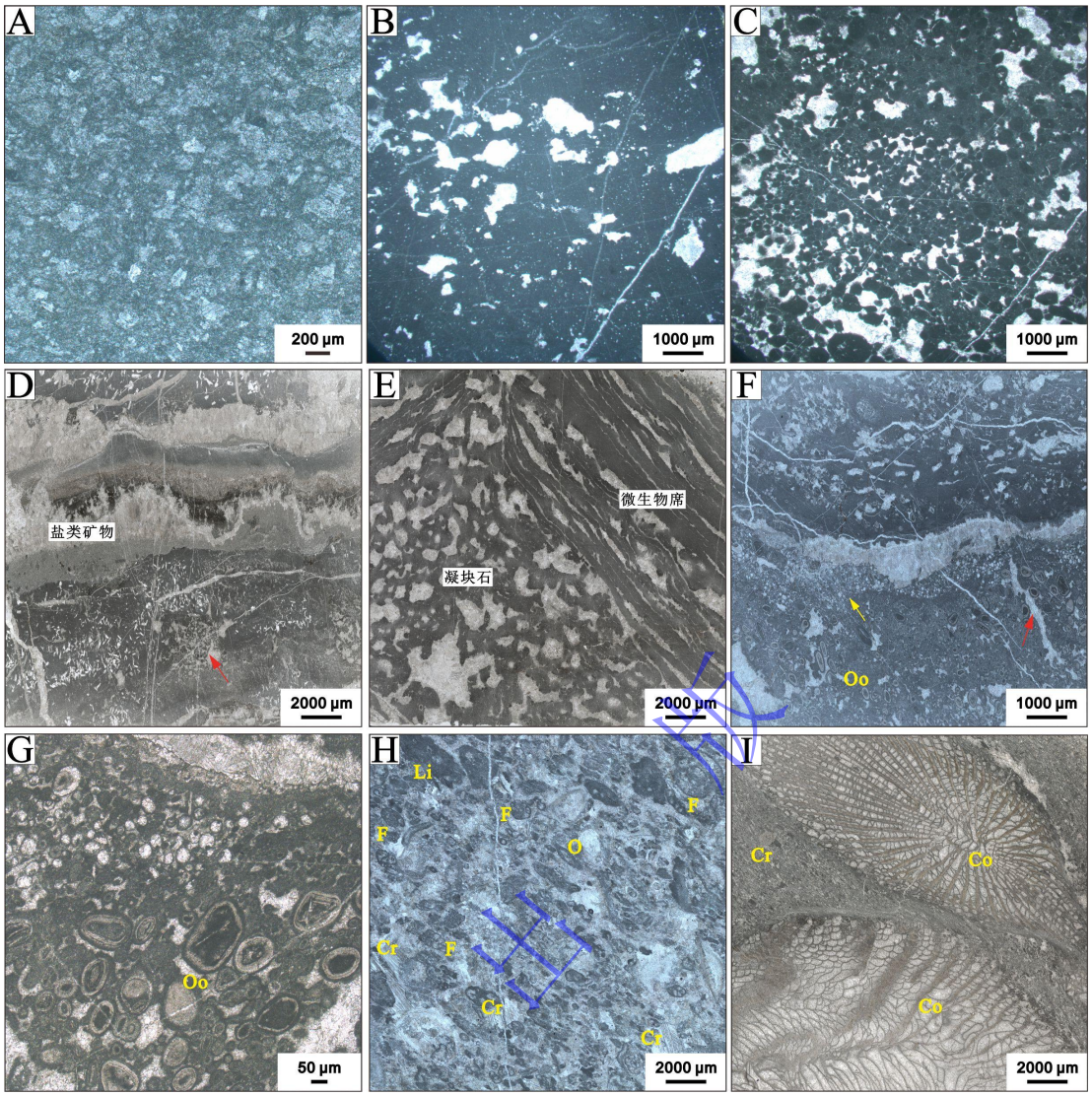

图 5 水峒剖面局限台地相与开阔台地相典型微相照片

（A）白云岩化灰岩（Mf1），SDB-218，340.3 m；（B）泥晶灰岩（Mf2），发育不同规模的溶蚀孔，SDB-98，139.3 m；（C）含不规则的纹层状窗格构造的泥粒灰岩（Mf2），SDB-105，146.5 m；（D）含蒸发盐矿物的微生物岩（Mf3），可见石膏假晶（黄色箭头所指）和微生物成因组构（红色箭头所指），SDB-216，338 m；（E）具有凝块-微生物席复合组构的微生物岩（Mf3），SDB-260，383.8 m；（F）泥晶灰岩（Mf2）覆盖于含单晶鲕粒（黄色箭头）的泥粒灰岩（Mf4）之上，二者以沉积间断面所隔，注意在沉积间断面之下发育的植根构造（红色箭头所指），SDB-214，337 m；（G）图 F 局部放大，可见单晶鲕粒层之下的泥晶化鲕粒层，SDB-214，337 m；（H）泥粒灰岩（Mf5），SDB-140，205.9 m；（I）漂砾灰岩（Mf6），见完整的横板珊瑚，SDB-186，313.4 m。缩写含义：Oo-鲕粒；Cr-海百合；F-有孔虫；Li-内碎屑；O-介形虫；Co-珊瑚

Fig. 5 Microphotographs of typical microfacies from the restricted and open platform facies associations in the Shuidong section

(A) Dolomitized limestone (Mf1). SDB-218, 340.3 m; (B) Mudstone with dissolution pores of various sizes (Mf2). SDB-98, 139.3 m; (C) Packstone with laminated fenestral fabrics (Mf2). SDB-105, 146.5 m; (D) Microbialite containing abundant evaporite minerals (Mf3), with gypsum pseudomorphs and microbial-related fabrics highlighted by yellow and red arrows, respectively. SDB-216, 338 m; (E) Microbialite displaying both thrombolitic and stromatolitic fabrics (Mf3). SDB-260, 383.8 m; (F) A mudstone (Mf2) overlies a packstone (Mf4) containing monocrystalline ooids (indicated by the yellow arrow), with the two lithologies separated by a sedimentary discontinuity. Note the root structure developed beneath the discontinuity (indicated by the red arrow). SDB-214, 337 m; (G) A close-up view of local figure 4F, showing a micritized ooid layer underlying the monocrystalline ooid layer. SDB-214, 337 m; (H) Packstone (Mf5). SDB-140,

205.9 m; (I) Floatstone containing whole tabulate corals (Mf6). SDB-186, 313.4 m. Abbreviations: Oo-Ooid; Cr-Crinoid; F-Foraminifer; Li-Litholacst; O-Ostracod; Co-Coral

Mf9：似球粒泥粒—颗粒灰岩。该微相以含丰富的似球粒为特征（图 6E），也见腕足、腹足、海百合、苔藓虫和有孔虫等生物碎屑颗粒。颗粒通常分选性较差，粒径范围可达 200~2 500 μm，与传统的滩相颗粒灰岩存在较大差别（Tucker and Wright，2009）。因此，该微相可能形成于颗粒滩后浅水潮下带环境，位于正常天气浪基面之上或附近（Hüneke *et al.*，2001；Amirshahkarami *et al.*，2007）。

4.3 边缘颗粒滩相组合

Mf10：鲕粒灰岩。该微相宏观上表现为巨厚层的鲕粒灰岩（图 4H），镜下以含分选性较好的同心鲕粒和少量似球粒为特征（图 6F）。鲕粒类型主要包括正常鲕和表鲕（图 6G），偶见破碎鲕，其核心多为似球粒和细小的生物碎屑。传统观点认为，鲕粒形成于碳酸盐过饱和、水动力较强的浅水动荡环境（Harris，1979；Diaz and Eberli，2019；李飞等，2024）。因此，该微相形成于水动力较强的台地边缘颗粒滩环境（Palma *et al.*，2007；Fügel，2010）。

Mf11：生物碎屑颗粒灰岩。该微相宏观上表现为巨厚层的生物碎屑颗粒灰岩（图 4I）。颗粒以海百合、腕足、有孔虫、腹足和藻类等生物碎屑为主，也含似球粒、内碎屑、鲕粒等非生物组分（图 6H）。碎屑颗粒整体分选和磨圆度较好，反映其形成于高水动能沉积环境（Tucker and Wright，2009）。该微相沉积于台地边缘颗粒滩（Blomeier *et al.*，2009）。

4.4 上斜坡相组合

Mf12：生物碎屑砾屑灰岩。该微相宏观上存在显著的粒序层理（图 4J），镜下可见内碎屑、似球粒、海百合、腕足、有孔虫和腹足等碎屑颗粒，磨圆度中等，分选性较差（图 6I）。这些特征表明该微相形成于滩前上斜坡环境（Bahamonde *et al.*，2004；Reijmer *et al.*，2012），位于正常天气浪基面和风暴浪基面之间（Hüneke *et al.*，2001）。

综上所述，早石炭世中晚期水峒剖面经历了局限台地、开阔台地、台地边缘生物碎屑颗粒滩和上斜坡环境（图 7）。巴马台地北缘与南缘极为相似，都发育有颗粒滩（Liu *et al.*，2015；刘超，2017）。因此，巴马台地此阶段属于具镶边结构的孤立碳酸盐岩台地。

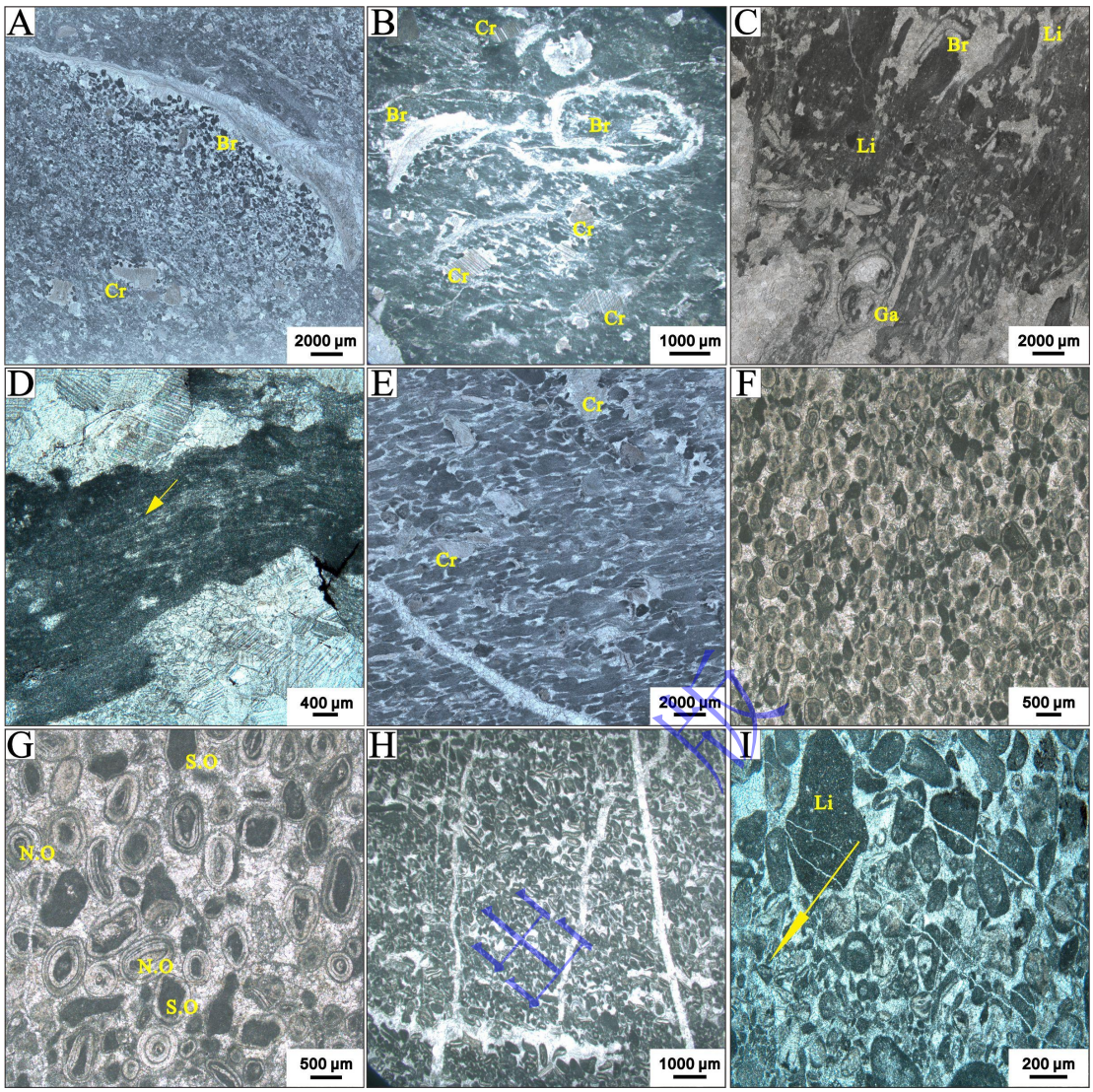

图 6　水峒剖面开阔台地相、颗粒滩相及上斜坡相典型微相照片

（A）含腕足介壳的漂砾灰岩（Mf7），介壳凸面向上，SDB-147，218.6 m；（B）含腕足介壳的漂砾灰岩（Mf7），介壳多凸面向上，SDB-262，383.8 m；（C）含凝块组构的粒泥灰岩（Mf8），SDB-263，384.2 m；（D）含凝块组构的粒泥灰岩（Mf8），可见管状钙化蓝细菌（黄色箭头所指），SDB-263，384.2 m；（E）分选较差的似球粒颗粒灰岩（Mf9），SDB-191，317.6 m；（F）鲕粒灰岩（Mf10），SDB-242，361.1 m；（G）鲕粒灰岩（Mf10），鲕粒多为同心的正常鲕和表鲕，SDB-237，357.4 m；（H）生物碎屑颗粒灰岩（Mf11），SDB-241，360.2 m；（I）砾屑灰岩（Mf12），可见明显的粒序层理（黄色箭头方向所指），SDB-234，355 m。缩写含义：Br-腕足；Cr-海百合；Li-内碎屑；Ga-腹足；N.O-正常鲕；S.O-表鲕

Fig. 6 Microphotographs of typical microfacies from the open platform facies, shoal, and upper slope facies associations in the Shuidong section

(A) Floatstone containing convex-up brachiopod shells (Mf7), SDB-147, 218.6 m; (B) Floatstone containing mostly convex-up brachiopod shells (Mf7), SDB-262, 383.8 m; (C) Thrombolitic wackestone (Mf8), SDB-263, 384.2 m; (D) Thrombolitic wackestone containing tubular calcified cyanobacterial fossils (indicated by the yellow arrow) (Mf8), SDB-263, 384.2 m; (E) Poorly-sorted peloidal grainstone (Mf9), SDB-191, 317.6 m; (F) Oolitic limestone (Mf10), SDB-242, 361.1 m; (G) Oolitic limestone, with predominantly concentric normal and superficial ooids (Mf10), SDB-237, 357.4 m; (H) Bioclastic grainstone (Mf11), SDB-241, 360.2 m; (I) Rudstone showing normal graded bedding (indicated by the yellow arrow) (Mf12), SDB-234, 355 m; Abbreviations: Br-Brachiopod; Cr-Crinoid; Li-Lithoclast; Ga-Gastropod; N.O-Normal Ooid; S.O -Superficial Ooid

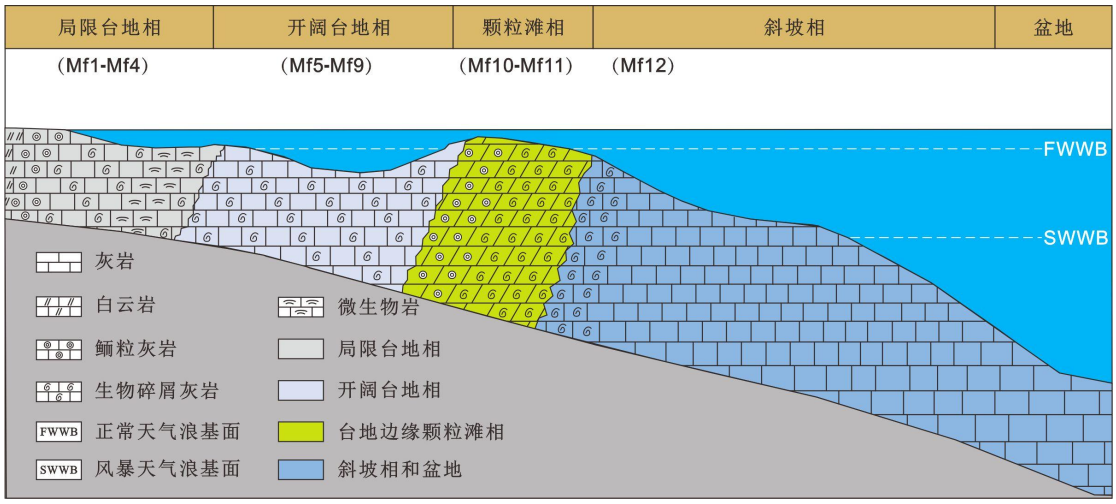

图 7 早石炭世中晚期巴马孤立台地北缘沉积模式图（修改自刘超，2017）

FWWB 为正常天气浪基面，SWWB 为风暴浪基面

Fig.7 A depositional model of the northern Bama isolated platform during the middle-late Early Carboniferous (modified after Liu, 2017)

FWWB denotes the Fair-Weather Wave Base, whereas SWWB denotes the Storm-Weather Wave Base

表 1 水峒剖面都安组微相特征及环境解释

Table 1 Microfacies characteristics and environmental interpretations of the Du'an Formation in the Shuidong section

沉积相组合	微相类型	结构	构造	主要颗粒类型	环境解释
局限台地相组合	Mf1	白云岩	—	含半自形白云石晶体，无生物碎屑	潮上带
	Mf2	泥晶—泥粒灰岩	窗格构造	常见似球粒	潮上带至潮间带
	Mf3	微生物岩	凝块状、叠层状构造	常见蒸发盐矿物，如石膏假晶	潮上带至潮间带
	Mf4	泥粒灰岩	植根构造	含丰富的单晶鲕和泥晶化鲕粒	潮上带至潮间带
开阔台地相组合	Mf5	泥粒灰岩		含丰富的有孔虫和海百合，常见介形虫、腕足、藻类、似球粒和内碎屑等	潮下带上部，FWWB 之上
	Mf6	漂砾灰岩	—	含完整的珊瑚或腕足化石，常见似球粒、内碎屑、有孔虫、海百合、腹足、双壳和藻类等	潮下带下部，FWWB 之下
	Mf7	漂砾灰岩	—	为腕足介壳层，含丰富且较大的腕足介壳，常见棘皮、腹足等	潮下带下部，FWWB 与 SWWB 之间
	Mf8	粒泥灰岩	凝块状构造	常见似球粒、内碎屑、腕足、海百合和腹足等	深水潮下带，FWWB 之下
	Mf9	泥粒—颗粒灰岩	—	含丰富的似球粒和内碎屑，常见腕足、腹足、钙球、海百合、苔藓虫、介形虫和有孔虫等	潮下带上部，FWWB 之上或附近
颗粒滩相组合	Mf10	鲕粒灰岩	—	含丰富的鲕粒，常见似球粒	台地边缘颗粒滩
	Mf11	生物碎屑颗粒灰岩	—	含丰富的似球粒和内碎屑，常见藻类、海百合、腕足、腹足、有孔虫、钙球、包粒和内碎屑，偶见双壳	台地边缘颗粒滩
上斜坡相组	Mf12	砾屑灰岩	粒序层理	含丰富的似球粒和内碎屑，常见鲕粒、腕足、海百合、	边缘滩前上斜坡，

5 水峒剖面下石炭统海侵—海退旋回对晚古生代大冰期主幕启动的响应

作为层序地层学重要的理论基石之一，海侵—海退旋回（Johnson and Murphy，1984；Johnson *et al.*，1985）或海侵—海退层序（Embry and Johannessen，1993）是进行盆地、区域和全球尺度地层对比的有效工具（Catuneanu *et al.*，2009；Qiu *et al.*，2014；吴和源，2017）。一个完整的海侵—海退旋回包括一个海侵体系域和一个海退体系域，两者以最大海泛面为界，而旋回或层序界面由不整合暴露面和最大海退面共同组成（Embry，1993）。依据海侵—海退旋回理论，同时根据都安组沉积微相堆积序列及其横向特征（图 8），在右江盆地巴马台地水峒剖面维宪阶上部至谢普霍夫阶（Aleksinian 亚阶至 Zapultyubian 亚阶）共识别出 7 个海侵—海退旋回（图 8）。参考 Aretz *et al.*（2020）的年代地层格架，基于各亚阶的时间跨度，可得出每个旋回的持续时间（虽然部分旋回可能被不整合面改造，周期统计存在一定误差）。通过计算可知，维宪阶上部 3 个旋回（TR1—TR3）持续时间为 1.4~2.0 Ma，谢普霍夫阶 4 个旋回（TR4—TR7）持续时间为 1.1~3.0 Ma（图 9）。因此，这 7 个海侵—海退旋回属于三级层序（Catuneanu *et al.*，2009）。考虑到它们在时间跨度和旋回数量上与安徽巢湖凤凰山剖面（盛青怡等，2013）和贵州雅水剖面（Chen *et al.*，2019）具有很好的可对比性，右江盆地水峒剖面沉积旋回记录倾向于代表华南区域特征。

前人研究认为，低纬地区时间尺度小于 0.5 Myr、幅度大于 20 m 的海平面变化可反映受高纬冰川活动的影响（Rygel *et al.*，2008；Fielding，2021；Montañez，2022）。华南右江盆地水峒剖面都安组 7 个三级层序至少包含 26 个四级海侵—海退旋回（图 8，图 9）。维宪阶 TR1 由 2 个四级海侵—海退旋回组成，平均周期约为 0.75 Ma；TR2 由 4 个四级海侵—海退旋回组成，平均周期约为 0.5 Ma；TR3 至少由 3 个四级海侵—海退旋回组成，平均周期不高于 0.5 Ma。谢普霍夫阶 4 个三级层序由 17 个四级海侵—海退旋回组成，平均周期约为 0.45 Ma。类比现代及深时相似的碳酸盐沉积体系，假设巴马台地正常天气浪基面海水深度为 20~30 m（Immenhauser and Scott，2002；Immenhauser，2009），根据水峒剖面沉积相堆积序列和恢复的相对海平面变化曲线（图 10），认为右江盆地大幅度相对海平面变化（>20 m）开始于 Aleksinian 亚阶与 Mikhailovian 亚阶之交（即 TR1 顶部），表现为水峒地区从台地边缘颗粒滩—滩后浅水潮下带—深水潮下带—潮间带上部的快速相变。综上所述，华南右江盆地高频高幅海平面变化信号始于 Aleksinian-Mikhailovian 期之交，极有可能是对晚古生代大冰期主幕启动的响应。

除华南右江盆地外，北美和欧亚等低纬沉积序列中也普遍记录了类似的高频高幅海平面变化信号，但其初现时间存在明显差异（约 3~4 Ma，Aretz *et al.*，2020），主要包括三种情况（图 10）：Asbian 初期（英国，Wright and Vanstone，2001）、Asbian 晚期（等同于 Chesterian 初期或 Mikhailovian 初期；Cózar *et al.*，2023）（美国伊利诺斯盆地，Smith and Read，2000；美国阿巴拉契亚盆地，Al-Tawil and Read，2003；爱尔兰，Gallagher *et al.*，2006；美国内华达，Bishop *et al.*，2009；加拿大，Giles，2009；莫斯科盆地，Kabanov *et al.*，2016）和 Asbian-Brigantian 期之交（苏格兰，Fielding and Frank，2015）。如此之大的差异曾一度让部分学者认为，晚古生代大冰期可能不存在统一的陆地冰川活动启动时间（Aretz *et al.*，2020）。但根据近年来区域维宪阶—谢普霍夫阶年代地层最新的研究成果，笔者认为这种差异主要是原作者对地层年代解释的不确定性造成的。例如，精细的有孔虫生物地层和磁性地层研究表明，英国的高频旋回层初现于 Asbian 晚期，而非初期（Waters and Condon，2012；Cózar *et al.*，2022，2023；Hounslow *et al.*，2024）。在苏格兰东法夫地区，Brigantian 亚阶底界由 VF 孢粉组合带限定（Fielding and Frank，2015），但在英格兰坎布里亚 Brigantian 层型剖面，VF 孢粉带底界已划入 Asbian 晚期（McLean *et al.*，2018）。因此，与华南右江盆地记录一致，上述低纬沉积序列中高频高幅海平面变化信号均初现于 Aleksinian-Mikhailovian 期之交（等同于 Asbian 晚期或 Chesterian 初期），标志着晚古生代大冰期主幕的启动。值得一提的是，华南同期腕足壳$\delta^{18}O$记录（*C. panderi-E. ikensis* 有孔虫带底部）和爱尔兰磷酸盐化石$\delta^{18}O$记录（Cf6γ1 有孔虫带）均支持这一论断（图 10）：伴随 Aleksinian-Mikhailovian 期之交高频、高幅海平面变化信号的开始（亦即主幕的启动），古热带海洋海水表面温度急剧降低了约 4℃~5℃（Barham *et al.*，2012；Yao *et al.*，2022）（图 10）。

本研究提出的晚古生代大冰期主幕统一的启动时间（即 Aleksinian-Mikhailovian 期之交），为检验“晚古生代大冰期可能不存在统一的陆地冰川活动启动时间”假说的正确性及探究晚古生代大冰期主幕启动的驱动机制提供了关键约束。该启动时间的锚定，使区域和全球地质记录变化（代表地质事件）的发生时序形成了逻辑闭环。前人研究表明，在海西造山运动期间，低纬地区频繁的弧陆碰撞使大面积基性—超基性岩暴露地表（始于 335 Ma 前，即 Aleksinian 中期；Macdonald *et al.*，2019），这些幔源物质的风化速率很快，会消耗大气中大量 CO_2。同时，华南区域陆源输入也发生了同步增强（Liu *et al.*，2026b），表明全球维管植物的同步扩张（Xiong *et al.*，2013；Xue *et al.*，2015；Cascales-Miñana，2016）也是加快陆壳化学风化速率的重要诱因。陆壳化学风化会携带大量营养盐汇入海洋，刺激海洋表面初始生产力，进一步导致大气中大量 CO_2 被埋藏（Liu *et al.*，2026b）。因此，Aleksinian 中晚期

陆地和海洋的巨大碳汇，共同驱动了晚古生代大冰期主幕在 Aleksinian-Mikhailovian 期之交启动。

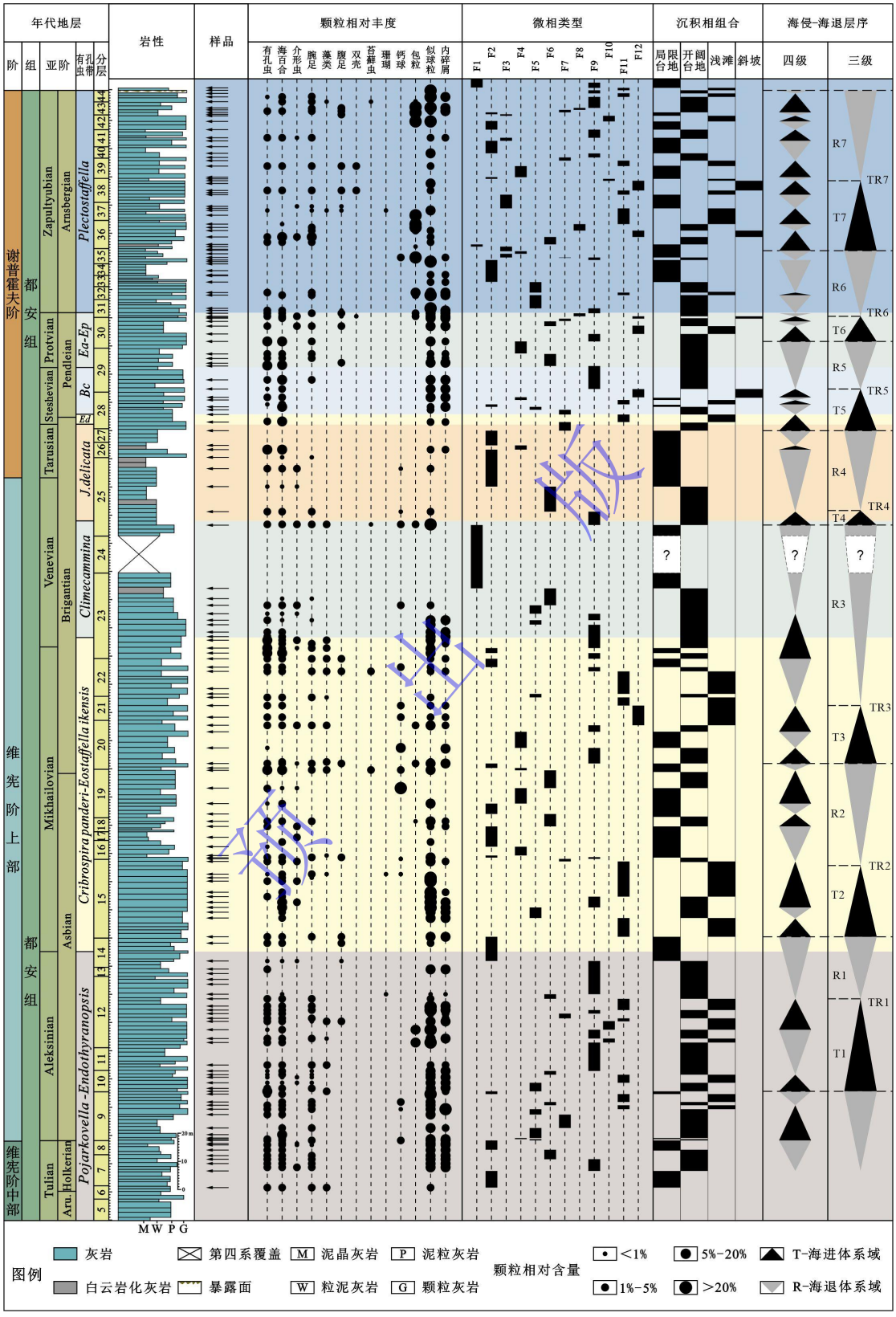

图 8 水峒剖面都安组沉积相和海侵—海退旋回综合柱状图

Fig.8 Comprehensive stratigraphic column illustrating sedimentary facies and transgressive-regressive cycles of the Du'an Formation at the Shuidong Section

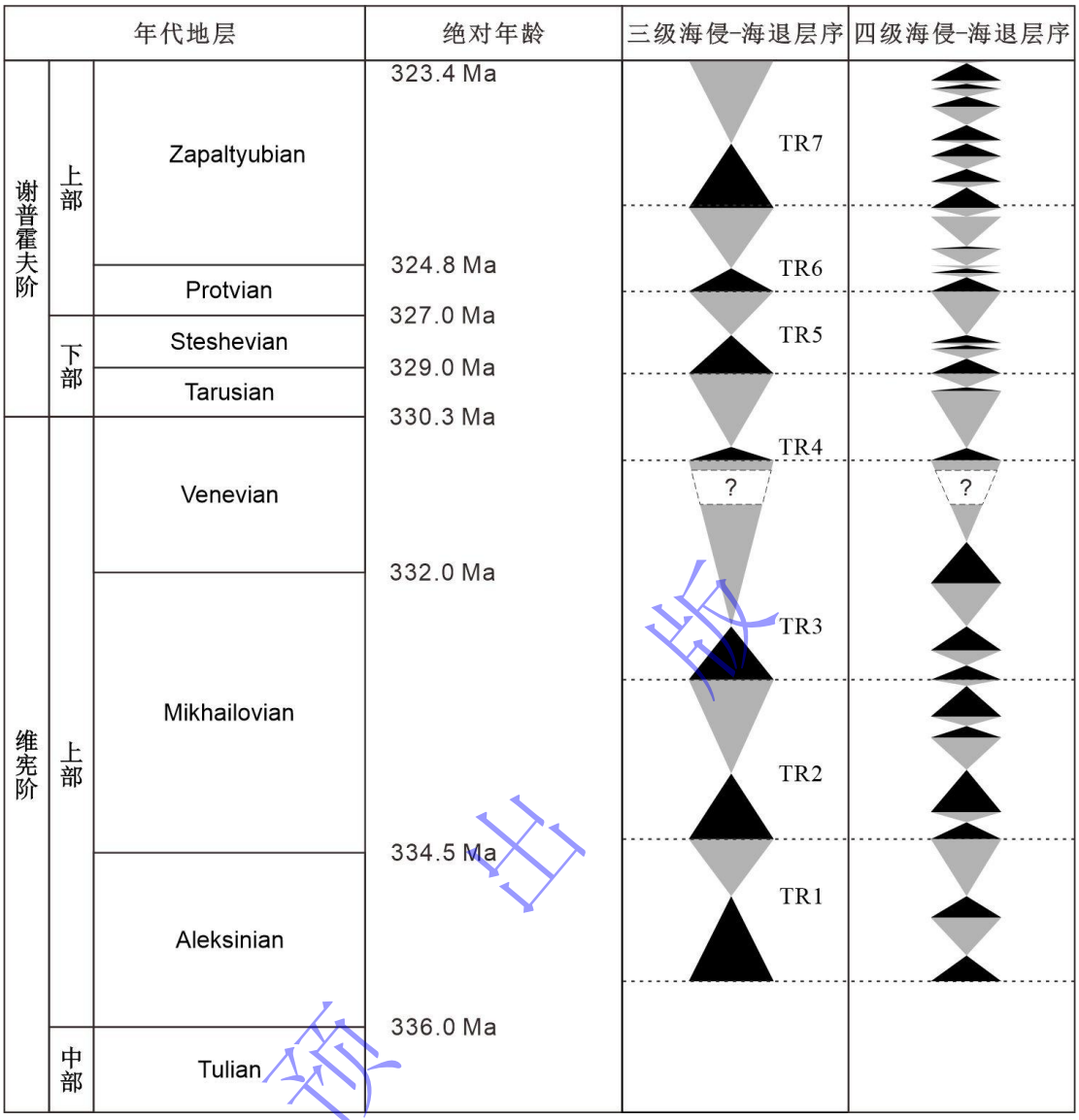

图 9 水峒剖面三级和四级海侵—海退旋回分布图（绝对年龄引自 Aretz *et al.*，2020）

Fig.9 Distribution of third- and fourth-order transgressive-regressive cycles at the Shuidong section (absolute ages from Aretz *et al.*，2020)

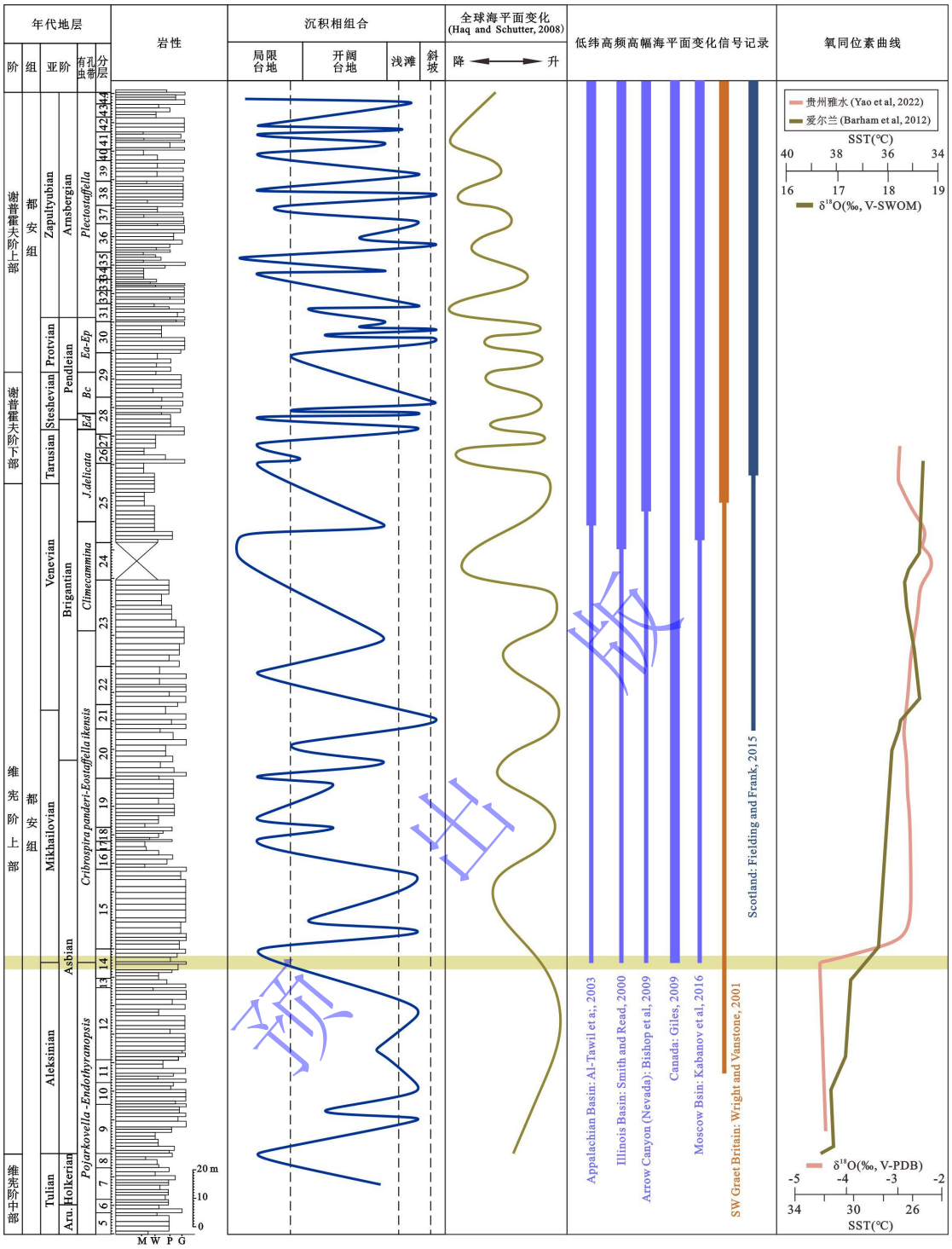

图 10 早石炭世中晚期右江盆地相对海平面变化与全球远程响应指标对比图

图中黄色阴影部分指示低纬高频高幅海平面变化初现层位及晚古生代大冰期主幕启动层位。全球海平面变化引自 Haq and Schutter，2008。不同区域海平面变化记录与氧同位素记录已校正到同一套年代地层格架下

Fig.10 Comparison of relative sea-level changes in the Youjiang Basin with global far-field proxies for the middle-late Early Carboniferous

The yellow-shaded interval denotes the stratigraphic level marking both the first occurrence of high-frequency, high-amplitude sea-level fluctuations and the onset of the main phase of the Late Paleozoic Ice Age. Global sea level changes cited from Haq and Schutter, 2008. Sea-level changes and oxygen isotope records from multiple geographic regions have been integrated into a unified chronostratigraphic framework

6 结论

（1）通过详细的沉积学分析，在华南右江盆地巴马孤立台地水峒剖面维宪阶中部至谢普霍夫阶顶部共识别出 12 种沉积微相类型，可进一步合并为 4 种沉积相组合类型，分别为局限台地相组合、开阔台地相组合、台地边缘颗粒滩相组合和上斜坡相组合。

（2）通过沉积相堆积序列及横向分布特征，在水峒剖面维宪阶上部和谢普霍夫阶共识别出 7 个三级海侵—海退层序和至少 26 个四级海侵—海退旋回。这些三级层序可与华南其他剖面进行很好的对比。

（3）右江盆地高频（<0.5 Ma）、高幅（>20 m）海平面变化初现于 Aleksinian-Mikhailovian 期之交，与低纬其他远程响应指标记录一致，表明晚古生代大冰期主幕启动于该时期。

致谢　感谢两位审稿专家提出的宝贵建设性意见，对本文水平的提升有很大帮助。

参考文献（References）

杜远生，黄虎，杨江海，等. 2013. 晚古生代—中三叠世右江盆地的格局和转换[J]. 地质论评，59（1）：1-11. [Du Yuansheng, Huang Hu, Yang Jianghai, et al. 2013. The Basin translation from Late Paleozoic to Triassic of the Youjiang Basin and its tectonic signification[J]. Geological Review, 59(1): 1-11.]

冯增昭，杨玉卿，鲍志东. 1999. 中国南方石炭纪岩相古地理[J]. 古地理学报，1（1）：75-86. [Feng Zengzhao, Yang Yuqing, Bao Zhidong. 1999. Lithofacies palaeogeography of the Carboniferous in South China[J]. Journal of Paleogeography, 1(1): 75-89.]

李飞，李雅兰，王曾俊，等. 2024. 现代鲕粒工厂特征及对深时研究的启示[J]. 沉积学报，42（2）：371-386. [Li Fei, Li Yalan, Wang Zengjun, et al. 2024. Modern ooid factories and clues to understanding their deep-time analogs[J]. Acta Sedimentologica Sinica, 42(2): 371-386.]

李儒峰，刘本培，赵澄林. 1997. 扬子板块石炭纪沉积层序及其全球性对比研究[J]. 沉积学报，15（3）：25-30. [Li Rufeng, Liu Benpei, Zhao Chenglin. 1997. Correlation of Carboniferous depositional sequences on the Yangtze Plate with others on a global scale[J]. Acta Sedimentologica Sinica, 15(3): 25-30.]

刘本培，李儒峰，尤德宏. 1994. 黔南独山石炭系层序地层及麦粒蜓带冰川型全球海平面变化[J]. 地球科学：中国地质大学学报，19（5）：553-564. [Liu Benpei, Li Rufeng, You Dehong. 1994. Carboniferous sequence stratigraphy and glacio-eustasy of *Triticites* Zone in South Guizhou, China[J]. Earth Science: Journal of China University of Geosciences, 19(5): 553-564.]

刘超，陆刚，张喜，等. 2014. 桂西北天峨孤立碳酸盐岩台地晚古生代沉积特征与演化[J]. 地质论评，60（1）：55-70. [Liu Chao, Lu Gang, Zhang Xi, et al. 2014. Sedimentary characteristics and evolutionary stages in Late Paleozoic of Tian'e isolated platform in Northwestern Guangxi[J]. Geological Review, 60(1): 55-70.]

刘超. 2017. 华南右江盆地晚古生代巴马孤立台地沉积特征与演化：对深时古气候演变的响应和启示[D]. 武汉：中国地质大学. [Liu Chao. 2017. Sedimentary features and evolution of the Late Paleozoic isolated Bama Platform in the Youjiang Basin: Responses to and implications for the deep-time climate change[D]. Wuhan: China University of Geosciences.]

刘萧萧，刘超，胡霞. 粗粒叠层石研究进展[J/OL]. 成都理工大学学报（自然科学版）. https://link.cnki.net/urlid/51.1634.N.20250312.2337.002. [Liu Xiaoxiao, Liu Chao, Hu Xia. The coarse-grained stromatolites: A review of the present state of research[J/OL]. Journal of Chengdu University of Technology (Science & Technology Edition). https://link.cnki.net/urlid/51.1634.N.20250312.2337.002.]

郄文昆，张雄华，杜远生，等. 2010. 华南地区下石炭亚系碳同位素记录及对晚古生代冰期的响应[J]. 中国科学：地球科学，40（11）：1533-1542. [Qie Wenkun, Zhang Xionghua, Du Yuansheng, et al. 2010. Lower Carboniferous carbon isotope stratigraphy in South China: Implications for The Late Paleozoic Glaciation[J]. Science China Earth Sciences, 40(11): 1533-1542.]

沈阳，王训练，李玉坤，等. 2020. 黔南上司地区石炭系有孔虫：兼论华南维宪阶有孔虫生物地层序列[J]. 地学前缘，27（6）：213-233. [Shen Yang, Wang Xunlian, Li Yukun, et al. 2020. Carboniferous foraminifers from the Shangsi area in southern Guizhou and the Visean foraminiferal succession in South China[J]. Earth Science Frontiers, 27(6): 213-233.]

盛青怡，郑全锋，吴祥和，等. 2013. 安徽巢湖石炭系和州组地层学和沉积学研究新进展[J]. 地层学杂志，37（1）：41-47. [Sheng Qingyi, Zheng Quanfeng, Wu Xianghe, et al. 2013. Biostratigraphic and sedimentological progress of the Carboniferous Hezhou Formation at Chaohu, Anhui province[J]. Journal of Stratigraphy, 37(1): 41-47.]

史晓颖，侯宇安，帅开业. 2006. 桂西南晚古生代深水相地层序列及沉积演化[J]. 地学前缘，13（6）：153-170. [Shi Xiaoying, Hou Yu'an, Shuai Kaiye. 2006. Late Paleozoic deep-water stratigraphic succession in central Youjiang Basin: Constraints on Basin evolution[J]. Earth Science Frontiers, 13(6): 153-170.]

宋英凡，王向东，李莹，等. 2024. 华南石炭纪中期白云岩地层分布及其形成模式[J]. 地质学报，98（2）：346-362. [Song Yingfan, Wang Xiangdong, Li Ying, et al. 2024. Distribution and causes of Mid-Carboniferous dolomitization in South China[J]. Acta Geologica Sinica, 98(2): 346-362.]

王向东，胡科毅，郗文昆，等. 2019. 中国石炭纪综合地层和时间框架[J]. 中国科学：地球科学，49（1）：139-159. [Wang Xiangdong, Hu Keyi, Qie Wenkun, et al. 2019. Carboniferous integrative stratigraphy and timescale of China[J]. Science China Earth Sciences, 49(1): 139-159.]

吴和源. 2017. 朝向层序地层学标准化：层序地层学研究的一个重要科学命题[J]. 沉积学报，35（3）：425-435. [Wu Heyuan. 2017. Towards the standardization of sequence stratigraphy: An important scientific proposition of sequence stratigraphy[J]. Acta Sedimentologica Sinica, 35(3): 425-435.]

要乐，黄璞，陈波. 2023. 晚泥盆世—密西西比亚纪植物水循环与生物礁耦合演化[J]. 科学通报，68（12）：1473-1486. [Yao Le, Huang Pu, Chen Bo. 2023. Coupled evolution between plant hydrologic cycle and organic reef from Late Devonian to Mississippian[J]. Chinese Science Bulletin, 68(12): 1473-1486.]

张海军，王训练，丁林，等. 2006. 陕西镇安西口石炭—二叠系界线剖面蜓类生物多样性与高频海平面变化[J]. 中国科学：地球科学，36（3）：233-241. [Zhang Haijun, Wang Xunlian, Ding Lin, et al. 2006. The species diversity of fusulinaceans and high-frequency sea-level changes in the Carboniferous-Permian boundary section at Xikou, Zhen'an County, Shaanxi province, China[J]. Science China Earth Sciences, 36(3): 233-241.]

仲钰天，陈吉涛，高彪，等. 2023. 晚古生代大冰期碳—水循环回顾与展望[J]. 科学通报，68（12）：1544-1556. [Zhong Yutian, Chen Jitao, Gao Biao, et al. 2023. Carbon-water cycles during the Late Paleozoic Ice Age: Reviews and prospects[J]. Chinese Science Bulletin, 68(12): 1544-1556.]

Ahern J P, Fielding C R. 2021. Carboniferous Manning Canyon Formation, northern Utah, USA: A carbonate-mud-dominated cyclothem motif recording the main onset of The Late Paleozoic Ice Age[J]. Sedimentary Geology, 418: 105903.

Aigbadon G O, Ocheli A, Ozulu G U, et al. 2024. Sedimentary: Carbonate microfacies and mineralogy of the southern Benue Trough and eastern Dahomey Basin, Nigeria[J]. Unconventional Resources, 4: 100082.

Alekseev A S, Nikolaeva S V, Goreva N V, et al. 2022. Russian regional Carboniferous stratigraphy[M]//Lucas S G, Schneider J W, Wang X D, et al. The Carboniferous timescale. London: Geological Society, Special Publications, 49-117.

Alsharhan A S, Kendall C G S C. 2003. Holocene coastal carbonates and evaporites of the southern Arabian Gulf and their ancient analogues[J]. Earth-Science Reviews, 61(3/4): 191-243.

Al-Tawil A, Read J F. 2003. Late Mississippian (Late Meramecian-Chesterian), glacio-eustatic sequence development on an active distal foreland ramp, Kentucky, U.S.A.[M]//Ahr W M, Harris P M, Morgan W A, et al. Permo-Carboniferous carbonate platforms and reefs. Tulsa: SEPM Society for Sedimentary Geology, 33-54.

Amirshahkarami M, Vaziri-Moghaddam H, Taheri A. 2007. Sedimentary facies and sequence stratigraphy of the Asmari Formation at chaman-Bolbol, Zagros Basin, Iran[J]. Journal of Asian Earth Sciences, 29(5-6): 947-959.

Aretz M, Herbig H G, Wang X D. 2020. The Carboniferous Period[J]. Geologic Time Scale, 2: 811-874.

Bahamonde J R, Kenter J A M, Della Porta G, et al. 2004. Lithofacies and depositional processes on a high, steep-margined Carboniferous (Bashkirian-Moscovian) carbonate platform slope, Sierra del Cuera, NW Spain[J]. Sedimentary Geology, 166(1/2):

145-156.

Barham M, Murray J, Joachimski M M, et al. 2012. The onset of the Permo-Carboniferous glaciation: Reconciling global stratigraphic evidence with biogenic apatite $\delta^{18}O$ records in the Late Visean[J]. Journal of the Geological Society, 169(2): 119-122.

Bishop J W, Montañez I P, Gulbranson E L, et al. 2009. The onset of mid-Carboniferous glacio-eustasy: Sedimentologic and diagenetic constraints, Arrow Canyon, Nevada[J]. Palaeogeography, Palaeoclimatology, Palaeoecology, 276(1/2/3/4): 217-243.

Blake B M, Beuthin J D. 2008. Deciphering the mid-Carboniferous eustatic event in the central Appalachian foreland Basin, southern West Virginia, USA[M]//Fielding C R, Frank T D, Isbell J L. Resolving the Late Paleozoic ice age in time and space. Boulder: Geological Society of America, 249-260.

Blomeier D, Scheibner C, Forke H. 2009. Facies arrangement and cyclostratigraphic architecture of a shallow-marine, warm-water carbonate platform: The Late Carboniferous Ny Friesland Platform in eastern Spitsbergen (Pyefjellet Beds, Wordiekammen Formation, Gipsdalen Group)[J]. Facies, 55(2): 291-324.

Boboye O A, Okon E E. 2014. Sedimentological and geochemical characterization of the Cretaceous strata of Calabar Flank, southeastern Nigeria[J]. Journal of African Earth Sciences, 99: 427-441.

Buggisch W, Joachimski M M, Sevastopulo G, et al. 2008. Mississippian $\delta^{13}C_{carb}$ and conodont apatite $\delta^{18}O$ records-their relation to the Late Palaeozoic Glaciation[J]. Palaeogeography, Palaeoclimatology, Palaeoecology, 268(3/4): 273-292.

Butts S H. 2005. Latest Chesterian (Carboniferous) initiation of Gondwanan glaciation recorded in facies stacking patterns and brachiopod paleocommunities of the Antler foreland Basin, Idaho[J]. Palaeogeography, Palaeoclimatology, Palaeoecology, 223(3/4): 275-289.

Cai J X, Zhang K J. 2009. A new model for the Indochina and South China collision during the Late Permian to the Middle Triassic[J]. Tectonophysics, 467(1/2/3/4): 35-43.

Caputo M V, dos Santos R O B. 2020. Stratigraphy and ages of four Early Silurian through Late Devonian, Early and Middle Mississippian glaciation events in the Parnaíba Basin and adjacent areas, NE Brazil[J]. Earth-Science Reviews, 207: 103002.

Cascales-Miñana B. 2016. Apparent changes in the Ordovician–Mississippian plant diversity[J]. Review of Palaeobotany and Palynology, 227: 19-27.

Catuneanu O, Abreu V, Bhattacharya J P, et al. 2009. Towards the standardization of sequence stratigraphy[J]. Earth-Science Reviews, 92(1/2): 1-33.

Cawood P A, Zhao G C, Yao J L, et al. 2018. Reconstructing South China in Phanerozoic and Precambrian supercontinents[J]. Earth-Science Reviews, 186: 173-194.

Chen B, Joachimski M M, Shen S Z, et al. 2013. Permian ice volume and palaeoclimate history: Oxygen isotope proxies revisited[J]. Gondwana Research, 24(1): 77-89.

Chen B, Joachimski M M, Wang X D, et al. 2016a. Ice volume and paleoclimate history of the Late Paleozoic Ice Age from conodont apatite oxygen isotopes from Naqing (Guizhou, China)[J]. Palaeogeography, Palaeoclimatology, Palaeoecology, 448: 151-161.

Chen B, Chen J T, Qie W, et al. 2021. Was climatic cooling during the earliest Carboniferous driven by expansion of seed plants?[J]. Earth and Planetary Science Letters, 565: 116953.

Chen J T, Montañez I P, Qi Y P, et al. 2016b. Coupled sedimentary and $\delta^{13}C$ records of Late Mississippian platform-to-slope successions from South China: Insight into $\delta^{13}C$ chemostratigraphy[J]. Palaeogeography, Palaeoclimatology, Palaeoecology, 448: 162-178.

Chen J T, Montañez I P, Qi Y P, et al. 2018. Strontium and carbon isotopic evidence for decoupling of pCO_2 from continental weathering at the apex of the Late Paleozoic glaciation[J]. Geology, 46(5): 395-398.

Chen J T, Sheng Q Y, Hu K Y, et al. 2019. Late Mississippian glacio-eustasy recorded in the eastern Paleo-Tethys Ocean (South China)[J]. Palaeogeography, Palaeoclimatology, Palaeoecology, 531: 108873.

Chesnel V, Samankassou E, Merino-Tomé Ó, et al. 2016. Facies, geometry and growth phases of the Valdorria carbonate platform (Pennsylvanian, northern Spain)[J]. Sedimentology, 63(1): 60-104.

Cózar P, Somerville I D. 2021. The Serpukhovian in Britain: Use of foraminiferal assemblages for dating and correlating[J]. Journal of the Geological Society, 178(3): jgs2020-170.

Cózar P, Somerville I D, Hounslow M W, et al. 2022. A Late Asbian (Mississippian) stratotype for England: Trowbarrow Quarry, Cumbria, UK[J]. Papers in Palaeontology, 8(3): e1451.

Cózar P, Somerville I D, Hounslow M W, et al. 2023. Algal diversity during the onset of the Late Paleozoic Ice Age in low-latitude basins of the western Palaeotethys[J]. Earth-Science Reviews, 246: 104596.

Diaz M R, Eberli G P. 2019. Decoding the mechanism of Formation in marine ooids: A review[J]. Earth-Science Reviews, 190: 536-556.

Dunham R J. 1962. Classification of carbonate rocks according to depositional texture[M]//Ham W E. Classification of carbonate rocks-a symposium. Tulsa: American Association of Petroleum Geologists Memoir, 108-121.

Embry A F. 1993. Transgressive-regressive (T-R) sequence analysis of the Jurassic succession of the Sverdrup Basin, Canadian Arctic Archipelago[J]. Canadian Journal of Earth Sciences, 30(2): 301-320.

Embry A F, Johannessen E P. 1993. T-R sequence stratigraphy, facies analysis and reservoir distribution in the uppermost Triassic-Lower Jurassic succession, western Sverdrup Basin, Arctic Canada[J]. Norwegian Petroleum Society Special Publications, 2: 121-146.

Eros J M, Montañez I P, Osleger D A, et al. 2012. Sequence stratigraphy and onlap history of the Donets Basin, Ukraine: Insight into Carboniferous icehouse dynamics[J]. Palaeogeography, Palaeoclimatology, Palaeoecology, 313-314: 1-25.

Eyles N. 1993. Earth's glacial record and its tectonic setting[J]. Earth-Science Reviews, 35(1/2): 1-248.

Fielding C R, Frank T D, Birgenheier L P, et al. 2008. Stratigraphic imprint of the Late Palaeozoic Ice Age in eastern Australia: A record of alternating glacial and nonglacial climate regime[J]. Journal of the Geological Society, 165(1): 129-140.

Fielding C R, Frank T D. 2015. Onset of the glacioeustatic signal recording Late Palaeozoic Gondwanan ice growth: New data from palaeotropical East Fife, Scotland[J]. Palaeogeography, Palaeoclimatology, Palaeoecology, 426: 121-138.

Fielding C R. 2021. Late Palaeozoic cyclothems-a review of their stratigraphy and sedimentology[J]. Earth-Science Reviews, 217: 103612.

Fielding C R, Frank T D, Birgenheier L P. 2023. A revised, Late Palaeozoic glacial time-space framework for eastern Australia, and comparisons with other regions and events[J]. Earth-Science Reviews, 236: 104263.

Frank T D, Birgenheier L P, Montañez I P, et al. 2008. Late Paleozoic climate dynamics revealed by comparison of ice-proximal stratigraphic and ice-distal isotopic records[M]//Fielding C R, Frank T D, Isbell J L. Resolving the Late Paleozoic ice age in time and space. Boulder: Geological Society of America, 331-342.

Fügel E. 2010. Microfacies of carbonate rocks: Analysis, interpretation and application[M]. 2nd ed. Berlin, Heidelberg: Springer.

Gallagher S J, MacDermot C V, Somerville I D, et al. 2006. Biostratigraphy, microfacies and depositional environments of Upper Viséan limestones from the Burren region, County Clare, Ireland[J]. Geological Journal, 41(1): 61-91.

Giles P S. 2009. Orbital forcing and Mississippian sea level change: Time series analysis of marine flooding events in the Viséan Windsor Group of eastern Canada and implications for Gondwana glaciation[J]. Bulletin of Canadian Petroleum Geology, 57(4): 449-471.

Goddéris Y, Donnadieu Y, Carretier S, et al. 2017. Onset and ending of the Late Palaeozoic ice age triggered by tectonically paced rock weathering[J]. Nature Geoscience, 10(5): 382-386.

Gregg J M, Sibley D F. 1984. Epigenetic dolomitization and the origin of xenotopic dolomite texture[J]. Journal of Sedimentary Research, 54(3): 908-931.

Grossman E L, Joachimski M M. 2022. Ocean temperatures through the Phanerozoic reassessed[J]. Scientific Reports, 12(1): 8938.

Haq B U, Schutter S R. 2008. A chronology of Paleozoic sea-level changes[J]. Science, 322(5898): 64-68.

Harris P M. 1979. Facies anatomy and diagenesis of a Bahamian ooid shoal[M]. Miami: Comparative Sedimentology Laboratory, University of Miami.

Heckel P H. 2008. Pennsylvanian cyclothems in Midcontinent North America as far-field effects of waxing and waning of Gondwana ice sheets[M]//Fielding C R, Frank T D, Isbell J L. Resolving the Late Paleozoic ice age in time and space. Boulder: Geological Society of America, 299-330.

Heckel P H. 2023. North American Midcontinent Pennsylvanian cyclothems and their implications[M]//Lucas S G, DiMichele W A, Opluštil S, et al. Ice ages, climate dynamics and biotic events: The Late Pennsylvanian world. London: Geological Society of London, 131-166.

Hounslow M W, Cózar P, Somerville I D, et al. 2024. Rock magnetic-based cyclic expression in Late Visean ramp carbonates and an astrochronology for the Late Asbian from Northwest England[J]. Paleoceanography and Paleoclimatology, 39(3): e2023PA004772.

Hu Z Y, Bialik O M, Hohl S V, et al. 2021. Response of Mg isotopes to dolomitization during fluctuations in sea level: Constraints on the hydrological conditions of massive dolomitization systems[J]. Sedimentary Geology, 420: 105922.

Huang W T, Maillet M, Zhang Y L, et al. 2020. The onset of the major glaciation of the LPIA: Record from South China[J]. International Journal of Earth Sciences, 109(1): 281-300.

Hüneke H, Joachimski M, Buggisch W, et al. 2001. Marine carbonate facies in response to climate and nutrient level: The Upper Carboniferous and Permian of Central Spitsbergen (Svalbard)[J]. Facies, 45(1): 93-135.

Immenhauser A, Scott R W. 2002. An estimate of Albian sea-level amplitudes and its implication for the duration of stratigraphic hiatuses[J]. Sedimentary Geology, 152(1/2): 19-28.

Immenhauser A. 2009. Estimating palaeo-water depth from the physical rock record[J]. Earth-Science Reviews, 96(1/2): 107-139.

Isbell J L, Miller M F, Wolfe K L, et al. 2003. Timing of Late Paleozoic glaciation in Gondwana: Was glaciation responsible for the development of northern hemisphere cyclothems?[M]//Chan M A, Archer A W. Extreme depositional environments: Mega end members in geologic time. Boulder: Geological Society of America, 5-24.

Joachimski M M, von Bitter P H, Buggisch W. 2006. Constraints on Pennsylvanian glacioeustatic sea-level changes using oxygen isotopes of conodont apatite[J]. Geology, 34(4): 277-280.

Johnson J G, Murphy M A. 1984. Time-rock model for Siluro-Devonian continental shelf, western United States[J]. GSA Bulletin, 95(11): 1349-1359.

Johnson J G, Klapper G, Sandberg C A. 1985. Devonian eustatic fluctuations in Euramerica[J]. GSA Bulletin, 96(5): 567-587.

Jones A T, Fielding C R. 2004. Sedimentological record of the Late Paleozoic glaciation in Queensland, Australia[J]. Geology, 32(2): 153-156.

Kabanov P B, Alekseev A S, Gibshman N B, et al. 2016. The Upper Viséan-Serpukhovian in the type area for the Serpukhovian Stage (Moscow Basin, Russia): Part 1. Sequences, disconformities, and biostratigraphic summary[J]. Geological Journal, 51(2): 163-194.

Kaiser S I, Aretz M, Becker R T. 2016. The global Hangenberg Crisis (Devonian-Carboniferous transition): Review of a first-order mass extinction[M]//Becker R T, Königshof P, Brett C E. Devonian climate, sea level and evolutionary events. London: Geological Society of London, 387-437.

Lakin J A, Marshall J E A, Troth I, et al. 2016. Greenhouse to icehouse: A biostratigraphic review of latest Devonian-Mississippian glaciations and their global effects[M]//Becker R T, Königshof P, Brett C E. Devonian climate, sea level and evolutionary events. London: Geological Society of London, 439-464.

Lehrmann D J, Chaikin D H, Enos P, et al. 2015. Patterns of Basin fill in Triassic turbidites of the Nanpanjiang Basin: Implications for regional tectonics and impacts on carbonate-platform evolution[J]. Basin Research, 27(5): 587-612.

Liu C, Jarochowska E, Du Y S, et al. 2015. Microfacies and carbon isotope records of Mississippian carbonates from the isolated Bama Platform of Youjiang Basin, South China: Possible responses to climate-driven upwelling[J]. Palaeogeography, Palaeoclimatology, Palaeoecology, 438: 96-112.

Liu C, Du Y S, Jarochowska E, et al. 2018. A major anomaly in the carbon cycle during the Late Cisuralian (Permian): Timing, underlying triggers and implications[J]. Palaeogeography, Palaeoclimatology, Palaeoecology, 491: 112-122.

Liu C, Cózar P, Coronado I, et al. 2023a. Foraminifers and conodonts in the Danlu section, South China: Implications for the Viséan-Serpukhovian boundary (Mississippian)[J]. Geological Magazine, 160(6): 1131-1143.

Liu C, Vachard D, Cózar P, et al. 2023b. New species and evolution of the foraminiferal family Janischewskinidae in the Middle-Upper Mississippian of South China[J]. Palaeontologia Electronica, 26(1): a2.

Liu C, Vachard D, Cózar P, et al. 2023c. Middle to Late Mississippian and Early Pennsylvanian foraminiferal zonal scheme of South China-a case study from the Youjiang Basin: Biostratigraphical and palaeobiogeographical implications[J]. Lethaia, 56(1): 1-23.

Liu C, Cózar P, Coronado I, et al. 2026a. A refined Middle-Late Mississippian chronostratigraphic framework established through biostratigraphy and chemostratigraphy in South China: Implications for redefining the base of the Serpukhovian Stage[J].

Earth-Science Reviews, 274: 105392.

Liu C, Qi J J, Cózar P, et al. 2026b. Coupled tectonic-climatic-oceanographic dynamics drove the evolution of foraminiferal diversity in South China during the Middle to Late Mississippian[J]. Palaeogeography, Palaeoclimatology, Palaeoecology, 684: 113528.

Lumsden D N, Caudle G C. 2001. Origin of massive dolostone: The Upper Knox model[J]. Journal of Sedimentary Research, 71(3): 400-409.

Ma Y, Zhang S, Guo T, et al. 2008. Petroleum geology of the Puguang sour gas field in the Sichuan Basin, SW China[J]. Marine and petroleum geology, 25(4-5): 357-370.

Macdonald F A, Swanson-Hysell N L, Park Y, et al. 2019. Arc-continent collisions in the tropics set Earth's climate state[J]. Science, 364(6436): 181-184.

Machel H G, Mountjoy E W. 1986. Chemistry and environments of dolomitization-a reappraisal[J]. Earth-Science Reviews, 23(3): 175-222.

Maharjan D, Jiang G Q, Peng Y B, et al. 2018. Paired carbonate-organic carbon and nitrogen isotope variations in Lower Mississippian strata of the southern Great Basin, western United States[J]. Palaeogeography, Palaeoclimatology, Palaeoecology, 490: 462-472.

Mathews A, Woods A, Oliver C. 1991. Spots before the eyes: New comparison charts for visual percentage estimation in archaeological materials[M]//Middleton A, Freestone I. Recent developments in ceramic petrology. London: British Museum, 211-263.

McLean D, Owens B, Bodman D J, et al. 2018. Miospores from the Brigantian stratotype section at Janny Wood, Cumbria[J]. Proceedings of the Yorkshire Geological Society, 62(2): 89-100.

Metcalfe I. 2013. Gondwana dispersion and Asian accretion: Tectonic and palaeogeographic evolution of eastern Tethys[J]. Journal of Asian Earth Sciences, 66: 1-33.

Mii H S, Grossman E L, Yancey T E. 1999. Carboniferous isotope stratigraphies of North America: Implications for Carboniferous paleoceanography and Mississippian glaciation[J]. Geological Society of America Bulletin, 111(7): 960-973.

Montañez I P, Poulsen C J. 2013. The Late Paleozoic ice age: An evolving paradigm[J]. Annual Review of Earth and Planetary Sciences, 41(1): 629-656.

Montañez I P. 2022. Current synthesis of the penultimate icehouse and its imprint on the Upper Devonian through Permian stratigraphic record[M]//Lucas S G, Schneider J W, Wang X D, et al. The Carboniferous timescale. London: Geological Society of London, 213-245.

Nance R D, Gutiérrez-Alonso G, Keppie J D, et al. 2010. Evolution of the Rheic ocean[J]. Gondwana Research, 17(2/3): 194-222.

Nemyrovska T I. 2017. Late Mississippian-Middle Pennsylvanian conodont zonation of Ukraine[J]. Stratigraphy, 14(1/2/3/4): 299-318.

Ning M, Lang X G, Huang K J, et al. 2020. Towards understanding the origin of massive dolostones[J]. Earth and Planetary Science Letters, 545: 116403.

Palma R M, López-Gómez J, Piethé R D. 2007. Oxfordian ramp system (La Manga Formation) in the Bardas Blancas area (Mendoza province) Neuquén Basin, Argentina: Facies and depositional sequences[J]. Sedimentary Geology, 195(3/4): 113-134.

Poletaev V I, Vdovenko M V, Shulga V F, et al. 2013. Chapter 7. Carboniferous System[J]. Stratigraphy of Upper Proterozoic, Paleozoic and Mesozoic of Ukraine, 1: 247-356.

Poty E, Devuyst F X, Hance L. 2006. Upper Devonian and Mississippian foraminiferal and rugose coral zonations of Belgium and northern France: a tool for Eurasian correlations[J]. Geological Magazine, 143(6): 829-857.

Qie W, Zhang J P, Luo G M, et al. 2023. Enhanced continental weathering as a trigger for the End-Devonian Hangenberg crisis[J]. Geophysical Research Letters, 50(11): e2022GL102640.

Qiu Z, Wang Q C, Zou C N, et al. 2014. Transgressive-regressive sequences on the slope of an isolated carbonate platform (Middle-Late Permian, Laibin, South China)[J]. Facies, 60(1): 327-345.

Reijmer J J G, Palmieri P, Groen R. 2012. Compositional variations in calciturbidites and calcidebrites in response to sea-level fluctuations (Exuma Sound, Bahamas)[J]. Facies, 58(4): 493-507.

Riding R. 2000. Microbial carbonates: The geological record of calcified bacterial-algal mats and biofilms[J]. Sedimentology, 47(S1): 179-214.

Riding R. 2011. Microbialites, stromatolites, and thrombolites[M]//Reitner J, Thiel V. Encyclopedia of geobiology. Dordrecht: Springer, 635-654.

Rygel M C, Fielding C R, Frank T D, et al. 2008. The magnitude of Late Paleozoic glacioeustatic fluctuations: A synthesis[J]. Journal of Sedimentary Research, 78(8): 500-511.

Sallam E S, Ruban D A, Van Loon A J T. 2022. Lagoonal carbonate deposition preceding rifting-related uplift: Evidence from the Bartonian-Priabonian (Eocene) of the northwestern Gulf of Suez (Egypt)[J]. Journal of Palaeogeography, 11(1): 8-30.

Scotese C R. 2021. An atlas of Phanerozoic paleogeographic maps: The seas come in and the seas go out[J]. Annual Review of Earth and Planetary Sciences, 49(1): 679-728.

Smith L B, Read J F. 2000. Rapid onset of Late Paleozoic glaciation on Gondwana: Evidence from Upper Mississippian strata of the Midcontinent, United States[J]. Geology, 28(3): 279-282.

Soreghan G S, Soreghan M J, Heavens N G. 2019. Explosive volcanism as a key driver of the Late Paleozoic Ice Age[J]. Geology, 47(7): 600-604.

Tucker M E, Wright V P. 2009. Carbonate sedimentology[M]. New York: Wiley.

Wang Q F, Yang L, Xu X J, et al. 2020. Multi-stage tectonics and metallogeny associated with Phanerozoic evolution of the South China Block: A holistic perspective from the Youjiang Basin[J]. Earth-Science Reviews, 211: 103405.

Wang X D, Hu K Y, Qie W, et al. 2019. Carboniferous integrative stratigraphy and timescale of China[J]. Science China Earth Sciences, 62(1): 135-153.

Wang Y J, Qian X, Cawood P A, et al. 2018. Closure of the East Paleotethyan Ocean and amalgamation of the eastern Cimmerian and Southeast Asia continental fragments[J]. Earth-Science Reviews, 186: 195-230.

Warren J. 2000. Dolomite: Occurrence, evolution and economically important associations[J]. Earth-Science Reviews, 52(1/2/3): 1-81.

Warren J K. 2010. Evaporites through time: Tectonic, climatic and eustatic controls in marine and nonmarine deposits[J]. Earth-Science Reviews, 98(3/4): 217-268.

Waters C N, Condon D J. 2012. Nature and timing of Late Mississippian to Mid-Pennsylvanian glacio-eustatic sea-level changes of the Pennine Basin, UK[J]. Journal of the Geological Society, 169(1): 37-51.

Wilson M A, Palmer T J. 1992. Hardgrounds and hardground faunas[M]. Aberystwyth: University of Wales, Aberystwyth, 1-131.

Wilson P A, Roberts H H. 1992. Carbonate-periplatform sedimentation by density flows: A mechanism for rapid off-bank and vertical transport of shallow-water fines[J]. Geology, 20(8): 713-716.

Wright V P, Vanstone S D. 2001. Onset of Late Palaeozoic glacio-eustasy and the evolving climates of low latitude areas: A synthesis of current understanding[J]. Journal of the Geological Society, 158(4): 579-582.

Xiong C H, Wang D M, Wang Q, et al. 2013. Diversity dynamics of Silurian–Early Carboniferous land plants in South China[J]. PLoS One, 8(9): e75706.

Xue J Z, Huang P, Ruta M, et al. 2015. Stepwise evolution of Paleozoic tracheophytes from South China: Contrasting leaf disparity and taxic diversity[J]. Earth-Science Reviews, 148: 77-93.

Yang B, Zhang X H, Qie W, et al. 2020. Variabilities of carbonate $\delta^{13}C$ signal in response to the Late Paleozoic glaciations, Long'an, South China[J]. Frontiers of Earth Science, 14(2): 344-359.

Yang J H, Cawood P A, Du Y S, et al. 2012. Detrital record of Indosinian mountain building in SW China: Provenance of the Middle Triassic turbidites in the Youjiang Basin[J]. Tectonophysics, 574-575: 105-117.

Yao L, Qie W, Luo G M, et al. 2015. The TICE event: Perturbation of carbon-nitrogen cycles during the mid-Tournaisian (Early Carboniferous) greenhouse-icehouse transition[J]. Chemical Geology, 401: 1-14.

Yao L, Aretz M, Li Y, et al. 2016. Gigantoproductid brachiopod storm shell beds in the Mississippian of South China: Implications for their palaeoenvironmental and palaeogeographical significances[J]. Geologica Belgica, 19(1/2): 57-67.

Yao L, Aretz M, Wignall P B, et al. 2020. The longest delay: Re-emergence of coral reef ecosystems after the Late Devonian extinctions[J]. Earth-Science Reviews, 203: 103060.

Yao L, Jiang G Q, Mii H S, et al. 2022. Global cooling initiated the Middle-Late Mississippian biodiversity crisis[J]. Global and Planetary

Change, 215: 103852.

Youssef M, Ismail A, El-Sorogy A. 2017. Paleoecology and paleobiogeography of Paleocene ostracods in Dineigil area, south western Desert, Egypt[J]. Journal of African Earth Sciences, 131: 62-70.

Zeng Y F, Liu W J, Cheng H D, et al. 1995. Evolution of sedimentation and tectonics of the Youjiang composite Basin, South China[J]. Acta Geologica Sinica-English Edition, 8(4): 358-371.

Zhong Y T, Chen J T, Liu S A, et al. 2025. Zinc isotope perspective on global carbon cycling during the onset of the Late Paleozoic icehouse[J]. Geology, 53(2): 99-104.

Lower Carboniferous Sedimentary Cycles in the Bama Platform of the Youjiang Basin: Responses to the Onset of the Main-phase of the Late Paleozoic Ice Age

LIU Chao, SHEN Chenyang, LI Xin, QI Junjun

School of Resources and Environment, Henan Polytechnic University, Jiaozuo, Henan 454003, China

Abstract: [Objectives] The middle to late Early Carboniferous witnessed profound reorganization of Earth's tectonic paleogeography, climate systems, marine environments, and ecosystems. Establishing the precise temporal sequence of these events is critical for elucidating the coupled interactions among Earth's spheres and systems during this major climate abrupt transition. To refine the initiation timing of the main-phase of the Late Paleozoic Ice Age (LPIA), **[Methods]** this study integrates high-resolution sedimentary facies and their stacking patterns analyses of the Du'an Formation in the Shuidong Section, Youjiang Basin, South China. A robust transgressive–regressive (T-R) sequence framework was established, enabling quantitative reconstruction of relative sea-level history for the basin during the middle-late Early Carboniferous. **[Results]** Twelve microfacies were identified across the section, spanning the middle Visean to upper Serpukhovian. These are grouped into four distinct facies associations: restricted platform, open platform, platform-margin shoal, and upper slope. Seven third-order sequences and at least twenty-six fourth-order T-R cycles were resolved within the upper Visean and Serpukhovian. **[Conclusions]** The onset of high-frequency, high-amplitude relative sea-level fluctuations in the Youjiang Basin coincides with the Aleksinian-Mikhailovian boundary. This is independently corroborated by other low-latitude far-field proxies, thereby providing robust stratigraphic evidence that the main-phase of the LPIA initiated during this interval.

Key words: Youjiang Basin; Late Paleozoic Ice Age; Sedimentary microfacies; Transgressive-regressive sequence; Foraminiferal zone

Foundation: National Natural Science Foundation of China, No.42572135, 42172120
Corresponding author: LIU Chao, E-mail: liuchao661030@126.com